12-1-1987

Final Report: Two Dimensional Computer Simulation of Bilateral Silicon Solar Cells

Gregory Benedict Lush
Purdue University

Jeffery L. Gray
Purdue University

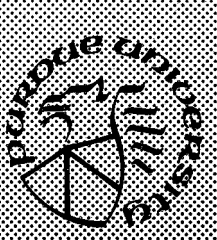

Final Report: Two Dimensional Computer Simulation of Bilateral Silicon Solar Cells

Gregory Benedict Lush
Jeffery L. Gray

TR-EE 87-37
October 1, 1985 - December 31, 1986

School of Electrical Engineering
Purdue University
West Lafayette, Indiana 47907

FINAL REPORT: TWO DIMENSIONAL COMPUTER SIMULATION OF BILATERAL SILICON SOLAR CELLS

by

Gregory Benedict Lush

and

Jeffery L. Gray

TR-EE-87-37

Project Period: October 1, 1985 to December 31, 1986

Supported by NASA-Lewis Research Center

ACKNOWLEDGMENTS

We would also like to thank B.L. Sater for many useful discussions and for experimental data used in this work.

This study was supported by NASA-Lewis Research Center Grant #NAG 3–657.

TABLE OF CONTENTS

Page

Page

LIST OF TABLES

Table Page

LIST OF FIGURES

Figure Page

Figure Page

LIST OF SYMBOLS

Symbol	Definition
A_n, A_p	Auger recombination coefficients for electrons, holes
AM0.0	Spectrum of light incident on solar cell in space
AM1.0	Spectrum of light incident on solar cell on earth
AM1.5	Spectrum of light used to simulate albedo light
BSF	Back surface field
EMVJ	Etched multiple vertical junction(solar cell)
EOL	End-of-life
η_c	Collection efficiency
F.F.	Fill factor
J_{dark}	Dark current
J_{mp}	Current at maximum power
J_o	Reverse saturation current
J_{sc}	Short circuit current
k	Boltzman's constant
K_l	Diffusion length damage Coefficient
$K_l(\rho)$	Diffusion length damage coefficient as a function of resistivity

Symbol	Definition
K_τ	Lifetime damage coefficient as a function of resistivity
L_n	Minority carrier diffusion length for electrons
L_o	Pre-irradiation diffusion length
n, p	Electron, hole concentration
n_1, p_1	Trap energy levels for electrons, holes
N_A	Acceptor doping concentration
N_C	Lifetime constant
N_D	Donor doping concentration
n_i	Intrinsic carrier concentration
Φ	Radiative fluence
Φ_A	Incident albedo energy
q	Electronic charge
R	Recombination rate
R_l	Load resistor of diode equivalent circuit
R_s	Series resistor of diode equivalent circuit
ρ	resistivity
SCAP2D	Solar cell analysis program in two dimensions
T	Temperature(Kelvin)
τ_{no}, τ_{po}	SCAP2D input lifetimes for electrons, holes
τ_n, τ_p	Electron, hole lifetimes
V_B	Voltage across diode base in equivalent circuit

Symbol	Definition
V_D	Voltage across diode in equivalent circuit
V_{mp}	Voltage at maximum power
V_{oc}	Open circuit voltage

ABSTRACT

Bilateral solar cells can convert albedo light (sunlight reflected from the earth) incident on the back side of the cell to improve the power to weight ratio of satellite arrays operating in Low Earth Orbits. However, the high energy radiation trapped in the Van Allen Belt surrounding the earth limits the possible improvement of solar cell electrical output by degrading the minority carrier diffusion length. The purpose of this work is to design cells to be able to collect efficiently albedo-generated carriers at end-of-life(EOL). The FORTRAN program Solar Cell Analysis Program in Two Dimensions is used to model four cell geometries for base resistivities of 1.0 to 1240. Ω–cm. The EOL efficiencies and normalized output power are compared for all cells. All the thicker (250. micron) cells modeled peak in performance within the 10.-40. Ω–cm base resistivity range both with and without albedo illumination. It is found that alternative geometries to the standard solar cell can be used to better collect albedo-generated carriers at EOL. The etched multiple vertical junction cell(22%) and the 50. micron thick standard cell(45%) show the most improvement in normalized output power over the best one-sun illuminated standard cell. Albedo light is modeled as 40. milliwatts/cm^2 (AM1.5 spectrum), or 30% of one sun AM0.0 incident power. Values for the damage coefficient, K_l, are found in the literature for irradiation by 1.0 MeV

electrons. Radiation induced degradation is modeled by SCAP2D through degradation of the minority carrier lifetimes. Solar cell output parameters are compared for four cells, the standard cell (for varying thicknesses), the etched multiple vertical junction cell, and the tandem junction cell. The physical phenomena responsible for poor cell performance at EOL are discussed.

CHAPTER 1

BILATERAL SOLAR CELLS FOR SPACE APPLICATIONS

1.1 The Problem

Satellites operating in Low Earth Orbits (LEO) suffer from increased torque on their span arms from the heavier atmosphere associated with LEO. Thus, it is useful to improve the power to weight ratio of the solar arrays operating on these satellites. To this end, the bilateral cell, which converts albedo (sunlight reflected from the earth) light from the earth as well as direct sunlight, is studied as a source of additional electrical power without additional weight.

The key limiting factor to solar cell efficiency in space is the high energy radiation trapped in the Van Allen Belt surrounding the earth. This radiation, made up of protons, neutrons, electrons, and ions, penetrates a cell and degrades the minority carrier diffusion length. Because the quantum efficiency of the solar cell is critically dependent on the diffusion length, radiation ultimately degrades the performance of solar cells. The ability of a cell to retain its initial efficiency while under radiative bombardment is referred to as the "hardness" of the cell to radiation.

Solar Cell Analysis Program in Two Dimensions (SCAP2D) [1] (Described in more detail in Appendix A.) models the performance of proposed solar

cells. SCAP2D simulates cells in an effort to find the geometries that make the best use of the albedo of the earth even after irradiation degrades the minority carrier diffusion length of solar cells.

Some important definitions that are incorporated into the text are described in the following section. A review of the report follows that section.

1.2 Definitions.

1.2.1 Albedo.

Albedo light is sunlight reflected off the earth back into space. This light can be converted to electrical energy by bilateral solar cells used in LEO. A bilateral cell is different from the standard front gridded solar cell in that the back contact is also gridded to allow collection of light on both surfaces. Sunlight is incident on the front of a solar cell and albedo light is incident on the back of the cell. Figure 1.1 shows the original standard cell and the bilateral standard cell as well as the etched multiple vertical junction (EMVJ) and tandem junction solar cells. The EMVJ and tandem junction designs result from changes made to the standard cell to improve albedo collection at end-of-life.

1.2.2 Radiation.

Radiation is high energy particles gravitationally trapped in the Van Allen Belt surrounding the earth. It is present in a wide spectrum of particles and energies that varies with changing orbit height. Radiation

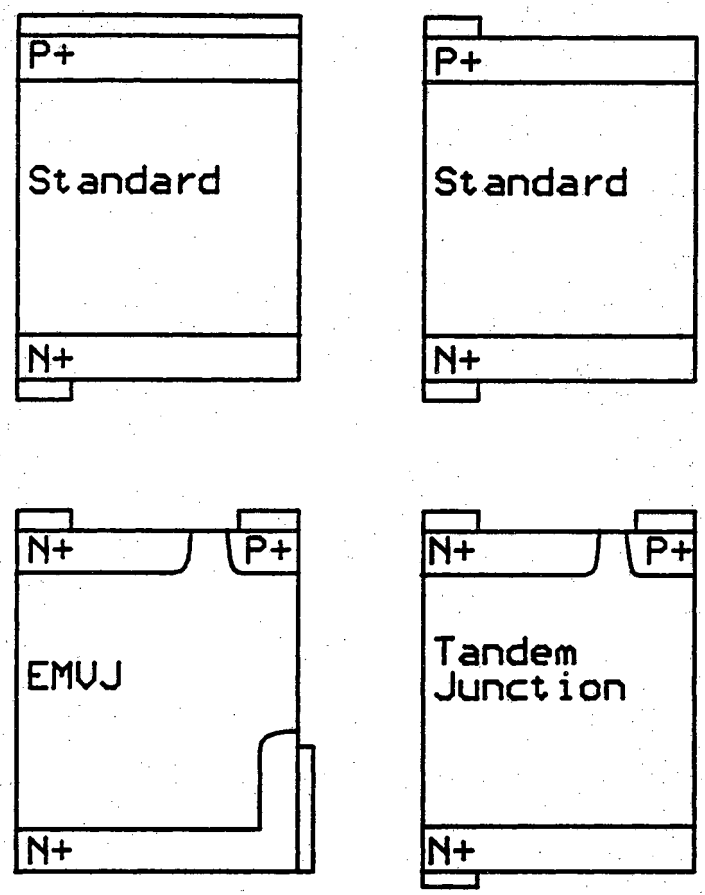

Figure 1.1 Four geometries simulated by SCAP2D: The standard cell, the bifacial standard cell, the tandem junction cell and the etched multiple vertical junction cell.

damages a solar cell lattice reducing the minority carrier diffusion length of that cell. Modeling the damage from this spectrum is difficult. Therefore, it is preferred to simplify the damaging effect of all radiation by use of the concept of equivalent fluence. An equivalent fluence is the total number per unit area incident of a monoenergetic particle needed to cause the same degree of damage as the spectrum of particles. Generally 1.0 MeV electrons are used. A linear relationship is assumed between time and the equivalent fluence incident on the cell. Figure 1.2 pictures the degradation of efficiency of a solar cell as a result of 1.0MeV electron equivalent fluence. (This plot is a cubic spline fit to data that are represented by the symbols. Most future plots of efficiency or output power are cubic spline fits as well.) It is important to note the difference between irradiation and illumination. Irradiation involves the high energy particles that damage the solar cell. Illumination is incident sunlight or albedo light that is converted to electrical energy by solar cells. End-of-life (EOL) refers to the end of a mission. A solar cell must be able to provide satisfactory power at EOL or the space vehicle will fail. Times for EOL will vary depending on the mission. The amount of radiative fluence that will be incident is dependent on orbit position and length of mission. Typically, 1.0e15 1.0MeV electrons/cm^2 is chosen as EOL for laboratory studies and it will be used here as well.

1.2.3 Cell Geometries.

Figure 1.1 shows all the cells and their respective geometries that are used in this work. The cells drawn represent unit cells of sorts. Each one is

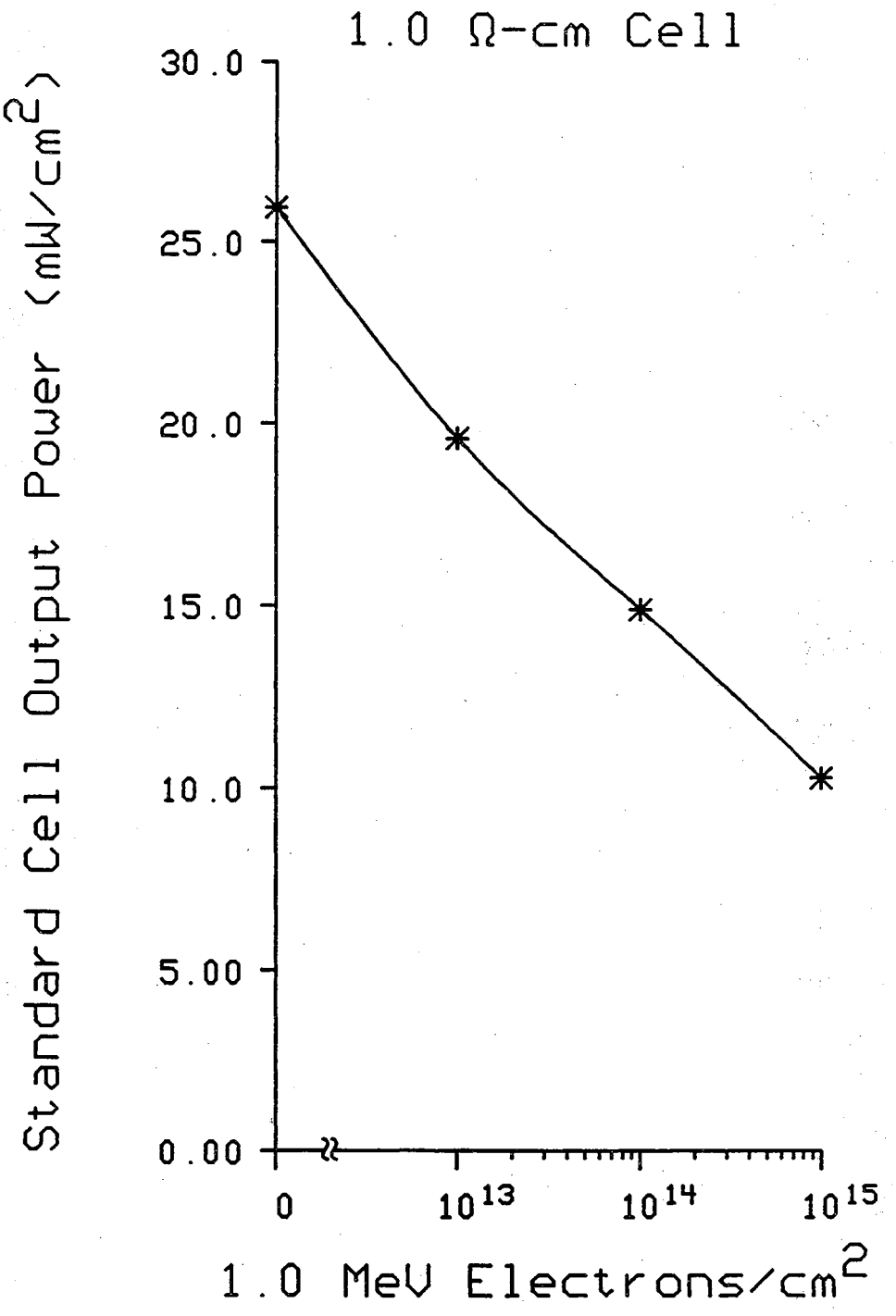

Figure 1.2 Degradation of the efficiency of a P-type standard solar cell.

the smallest possible representation of the cell to be simulated. In this way a large solar cell can be studied by simulating a small part of the entire cell. Tables 1.1 and 1.2 provide doping and length parameters for these cells. Figure 1.3 shows how a large solar cell is reduced to the smaller unit cell. The left and right sides of the reduced cells are lines of symmetry. Modeling the unit cell is the same as modeling the whole cell because so many unit cells are present that edge effects are negligible.

Table 1.1 Doping parameters for the four cells modeled.

BASE RESISTIVITIES(Ω-cm) AND BASE DOPING LEVELS(cm^{-3})						
1.0	2.0	10.	20.	40.	84.	1240
1.47e16	7.0e15	1.38e15	6.8e14	3.4e14	1.65e14	1.1e13

The standard cells in figure 1.1 can be N+PP+ structures or they can be P+NN+ structures. However, cells with P-type bases are always used because they are more radiation hard than similar cells with N-type bases [2]. Eventually, diffusion length degradation is so severe that collection of albedo-generated carriers by standard P-type cells ceases completely. The tandem junction cell incorporates a second emitter that is diffused into the albedo or back side of a standard cell. This additional emitter allows

Table 1.2 Geometric parameters for the four cells modeled.

INDIVIDUAL CELL PARAMETERS				
Parameter	Unilateral	Bilateral	Tandem	EMVJ
Thickness(μm)	250.	250.	250.	250.
Width(μm)	50.	50.	50.	50.
Emitter Doping(cm^{-3})	1.0e19	1.0e19	1.0e19	1.0e19
BSF Doping(cm^{-3})	1.0e19	1.0e19	1.0e19	1.0e19
X_j emitter(μm)	0.3	0.3	0.3	0.3
X_j BSF(μm)	1.0	1.0	1.0	1.0
BSF width(μm)	50.	50.	5.0	2.5
Albedo Emitter Width(μm)	--	--	40.	42.5
Surface Contacts(μm)	2.5/50.	2.5	2.5	2.5
Etched Contacts(μm)	--	--	--	100.

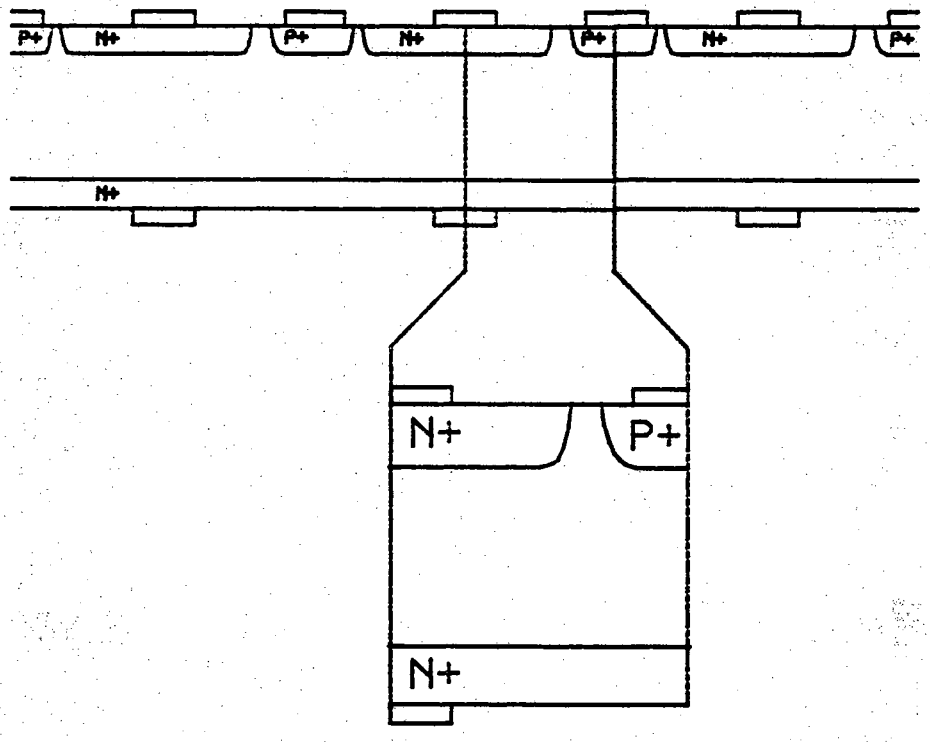

Figure 1.3 Reduction of a solar cell to a smaller unit cell.

collection of albedo carriers at EOL. The added emitter also increases shadowing on the albedo side since another contact is necessary. The etched multiple vertical junction (EMVJ) cell has etched front emitter contacts that collect carriers generated deep in the cell as well as at the surface. It is modeled as having no shadowing on the front side although some shadowing equal to the thickness of the contact is present. The EMVJ cell, like the tandem junction cell, has the additional contact and shadowing on the back side.

The specific base resistivities used in the computer simulations are chosen to correspond to values found in the literature. This is done to allow comparison between simulation results and published laboratory data. Appendix B details a comparison between published data and SCAP2D simulations.

There are many possible sources of error in the sequence of steps used to model the degradation of cell performance. Because of this, each individual efficiency or output power is less important than the trend that is seen among all resistivities. We are not trying to find precisely the EOL efficiencies of each cell. Rather, it is how each base resistivity and cell type does with respect to the others that is stressed.

1.3 Review of Report.

The goal of this work is to find solar cells best able to convert the additional illumination provided by albedo light into electrical energy at EOL. This requires modeling of the albedo light and the radiation-induced

degradation before SCAP2D modeling can begin.

Chapter 2 describes the characteristics and modeling of the albedo light. The intensity of the light is 40. milliwatts/cm^2, or 30% of one sun AM0.0 [3]. The light does not fit any of the standard spectrums (AM0.0, AM1.0, or AM1.5). However, it is assumed to be similar to the AM1.5 spectrum. Also, modifications to the standard cell are shown to be necessary. These modifications are needed because collection of albedo-generated carriers by standard cells ceases at EOL owing to diffusion length degradation.

Chapter 3 describes the procedure used to incorporate the degradation of minority carrier diffusion length into SCAP2D. It begins with an explanation of equivalent fluence. Equivalent fluence is then used to simplify the effects of doping on the damage coefficient, K_l, which is the measure of minority carrier diffusion length hardness to irradiation. The chapter concludes with an description of how irradiation is incorporated into SCAP2D as degraded minority carrier lifetimes.

The simulation results are reviewed in chapter 4. The EOL efficiencies and normalized output powers of the standard, tandem junction, and EMVJ solar cells are compared for base resistivities from 1.0 to 1240. Ω–cm. Normalized output power is the average output power delivered during the life of the cell. The structure of chapter 4 centers on the limits of improvement of cell efficiency. Each section studies how changing a specific parameter can improve cell performance. The peak of efficiency is located and the phenomena that limit the amount of improvement possible are then explained. Geometries other than those pictured in figure 1.1 were simulated, but each one failed to maintain a worthwhile efficiency. Only

those cells that showed strong radiation hardness are reported.

Chapter 5 provides conclusions and recommendations. The appendices explain in greater detail SCAP2D and some possible sources of error in the degradation models. Appendix B compares SCAP2D modeled degradation of cell output parameters to plots of the output parameters of laboratory degraded cells found in the literature.

CHAPTER 2

ALBEDO--DEFINITION AND CHARACTERISTICS

2.1 Introduction

The albedo of the earth is sunlight reflected off the earth back into space. This light can be converted to electrical energy by bilateral solar cells. This additional energy source can increase the power to weight ratio of solar arrays on low earth orbit (LEO) space vehicles. A bilateral solar cell incorporates gridded top contacts to collect light directly from the sun and gridded back contacts to collect albedo illumination incident on the back face. In this way, it is able to deliver more electrical power per cell than one that has light incident on the front side alone.

In this chapter, the characteristics of albedo light and its incorporation into SCAP2D are described. It will be shown that collection of the albedo generated carriers (which are mostly generated near the back surface) is made difficult by the harsh, radiative environment created by the Van Allen Belt. Redesign of the basic cell geometry is required to enable better collection of these additional carriers once radiation has reduced the diffusion length to shorter than the thickness of the cell. Finally, this chapter outlines the steps taken to alter the structure of the modeled bilateral cells so they can better collect the albedo light.

2.2 Albedo Characteristics

2.2.1 Albedo Spectrum.

Modeling the spectrum of albedo light presents some problems. The albedo spectrum varies with changes in the earth's appearance. This spectrum is dependent on the amount of light absorbed by the earth's atmosphere. Absorption is in turn determined by cloud cover, and the color changes associated with land and water. Thus, albedo light will have a varying spectrum certainly different from the standard spectrum models of AM0.0, AM1.0, or AM1.5. Some of the light will pass through the atmosphere twice, being reflected by land or water while some will penetrate a smaller distance, being reflected by cloud cover. By the definitions of the standard spectrums, the norm of this spectrum of light appears to be most like the AM1.5 spectrum. Thus, AM1.5 simulates the albedo incidence for SCAP2D solar cell modeling.

2.2.2 Incident Albedo Power.

The maximum power incident is 40.0 milliwatts/cm^2, AM1.5 [3], which is 30% of the power incident from the front side illumination of 135. milliwatts/cm^2, AM0.0. The actual power incident will change as a function of orbit, decreasing to zero over half the total orbit time. Figure 2.1 shows different orbit positions possible with the decreasing values of albedo intensity and θ, the angle from normal incidence associated with each position. We see that the full 40.0 milliwatt, AM1.5 maximum intensity will only be incident for a brief period of time, and that during half the orbit there is no albedo light. Some simulations will be performed at maximum

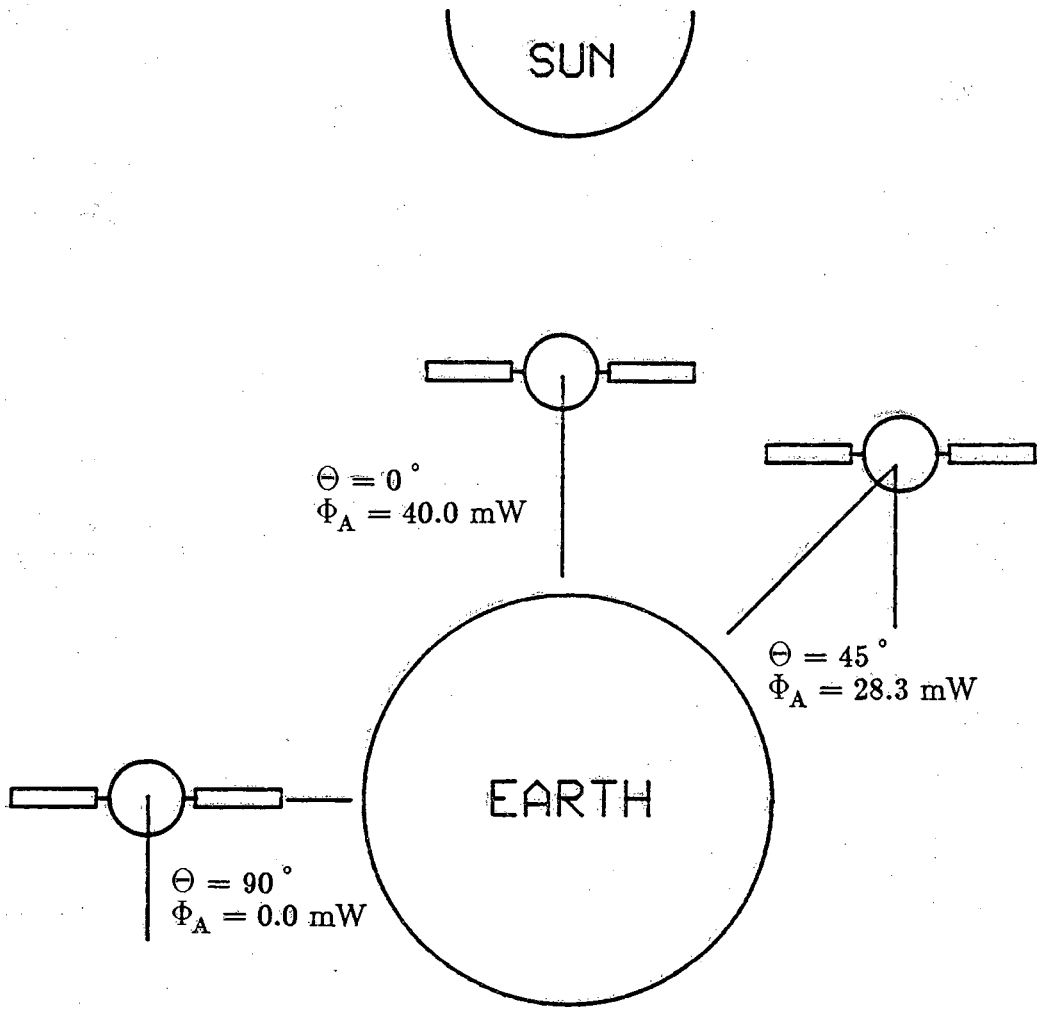

Figure 2.1 Orbit positions showing positions of weak albedo illumination.

albedo illumination, while others will be done without the benefit of albedo light for comparison since albedo light is not always available.

2.2.3 Benefits of Albedo Collection.

The need to make use of albedo light arises from satellites being employed in LEO. Here, an orbiter encounters a heavier atmosphere so that greater moments are generated on the array arms while in flight. To compensate, lighter arrays are needed without the orbiters suffering a loss of available power. With the collection of albedo light, the best high-resistivity thin (1240. Ω—cm, 50. microns thick) standard cell can produce up to 45.7% more power than the best (20. Ω—cm) 250. micron standard cell at EOL at maximum intensities. Because of this improvement, fewer cells are needed to provide the same amount of power. This results in possible reductions of the necessary weight of the arrays without suffering a loss of electrical power.

2.3 Changes In Cell Geometries

2.3.1 Loss of Albedo Collection For The P-type Standard Cell

Figure 1.1 shows how the standard P-type cell is changed to allow for collection of albedo generated carriers. In this figure are two identically doped cells--one of whose contacts was modified for albedo collection while the other was left unchanged. The latter does not receive albedo illumination. Tables 1.1 and 1.2 show doping and dimensional parameters of each cell. The back side of the original cell is covered by a contact.

Figure 2.2 shows the power output of each cell as a function of lifetime. Notice how the plots of each cell come together showing that all albedo collection has ceased. At this point the diffusion length is much shorter (125. microns) than the thickness of the cell. Thus, albedo generated electrons, which are mostly generated at the back surface, can no longer diffuse across the cell before being annihilated through recombination.

2.3.2 Tandem Junction and EMVJ Cells

To collect efficiently albedo-generated carriers, the cell requires an additional emitter junction added on the back surface. In this way, as the carriers are swept away from the surface by the surface—normal, built—in electric field, they are separated into regions in which the carriers are majority carriers. At this point, the carriers are collected. Figure 1.1 shows how the standard cell is changed into the tandem junction and the EMVJ cells to provide collecting junctions on the back side. Note, the new geometries double the albedo shadowing (from the back side contacts) over that of the standard bilateral cell because of the need for an additional contact on the N+ region. This reduces slightly the amount of albedo light the cell can collect.

Extending the emitter laterally on the EMVJ cell to completely cover the front surface is necessary for low lifetime collection of carriers. The N+ diffusions must cover as much of the incident surface as possible so that carriers drift away from the highly recombinative surface. Without a surface—normal, built—in electric field, surface recombination becomes the dominant carrier loss mechanism. Low lifetimes dictate that the

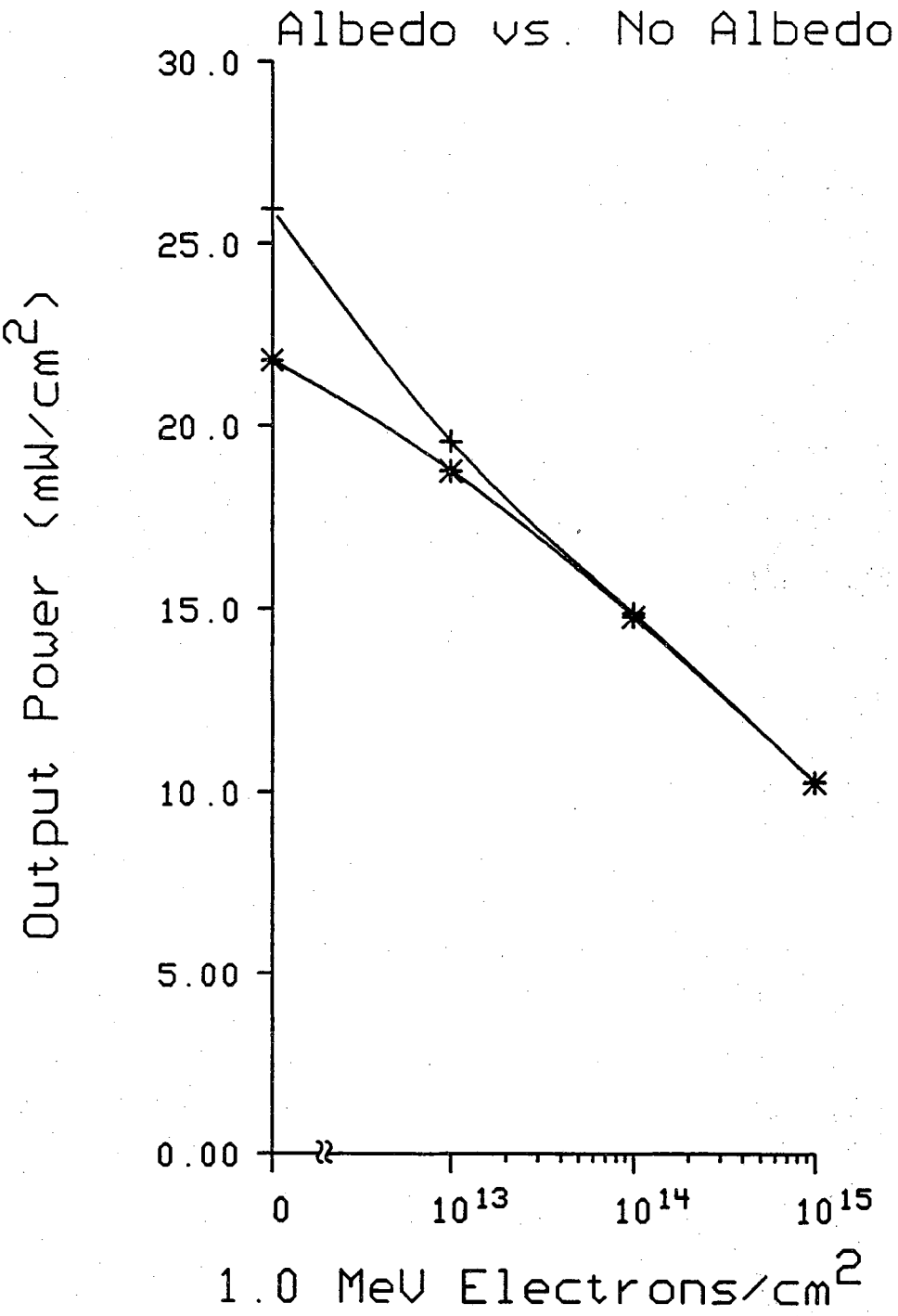

Figure 2.2 Demonstration of loss of albedo collection for 20.0 Ω—cm standard solar cell.

surface–normal electric field be an N+P collecting junction or the cell will approach zero efficiency because the BSF is not a collecting junction.

2.4 Conclusions

To review, the albedo is sunlight reflected from the earth back into space. This light is incident with a power of **40.0** milliwatts/cm^2, AM1.5 on the backs of solar cells operating in LEO. Exposing bilateral cells to this albedo light improves the output power of each cell. Therefore, smaller arrays can be used to provide the satellite with the same power. Modifications of the basic solar cell structure had to be made to efficiently collect the carriers generated by this back surface illumination at EOL. Low lifetime conditions dictate that emitter junctions should be used instead of BSF junctions on light-incident surfaces. Modifications to the standard cell resulted in the EMVJ and the tandem junction solar cell designs. These cells collect the albedo-generated carriers even after high energy particles trapped in the Van Allen Belt have reduced the base minority carrier lifetime. The result is a solar cell with improved electrical output that maintains large EOL efficiencies.

CHAPTER 3

MODELING RADIATION INDUCED DEGRADATION OF SOLAR CELL EFFICIENCY

3.1 Degradation of Solar Cell Output by Van Allen Radiation

High energy particles trapped in the Van Allen Belt surrounding the earth degrade the electrical performance of solar cells. These particles penetrate the cells, disrupt the ordered lattice, and introduce recombination centers. Recombination centers reduce the minority carrier diffusion length of the semiconductor material. Since cell performance is critically dependent on the minority carrier diffusion length, L_n, (L_n represents the minority carrier diffusion length in this chapter since most of the cells modeled are P-type.) radiation ultimately reduces the efficiency of the cell. This chapter describes the method used to model cell output degradation.

3.2 Introduction--Controlling Diffusion Length Degradation

The output parameters of all cells degrade to some degree in the harsh space environment because of L_n degradation. But proper choice of the geometry and doping parameters improve the ability of the cell to maintain its initial efficiency for a longer period of time. This ability is referred to as

the "hardness" of a cell to radiation. The degree of degradation of L_n is measured by the damage coefficient, K_l , which has the unit particles^{-1}. The smaller the value of K_l , the longer a cell can maintain its initial bulk diffusion length versus incident fluence.

A review of the L_n degradation model is the first section of this chapter. Then, to quantize the diffusion length degradation, space radiation is replaced with a monoenergetic equivalent fluence of 1.0MeV electrons. Following this, the effects of doping on the magnitude of K_l are reviewed. K_l, is a measure of diffusion length "hardness" to irradiation and is assumed to be only a function of resistivity. Next, an empirical formula for calculating $K_l(\rho)$ given a P-type base resistivity is found using literature data. Finally, the degradation of L_n is incorporated into SCAP2D to model the degradation of cell output. Also included is the handling of the surface recombination velocity, S, and its inclusion in the degradation model.

3.3 The Degradation Model

3.3.1 Diffusion Length Degradation Equation

An equation governing degradation of minority carrier diffusion length is given by

$$\frac{1}{L^2} = \frac{1}{L_o^2} + K_l(\rho)\Phi \qquad (3.1)$$

L is the diffusion length after Φ radiation, and L_o is the original diffusion length. The corresponding equation for degradation of minority carrier lifetime is as follows:

$$\frac{1}{\tau} = \frac{1}{\tau_o} + K_\tau(\rho)\Phi \tag{3.2}$$

With equations 3.1 and 3.2 a specific minority carrier diffusion length or lifetime can be found for a desired fluence of electrons. However, data for $K_l(\rho)$ is much more readily available in literature than for $K_\tau(\rho)$. Therefore, equation 3.1 is used with equation 3.3 below to find degraded minority carrier lifetimes.

$$\tau = \frac{q}{kT}\frac{L^2}{\mu} \tag{3.3}$$

Here, τ is the minority carrier lifetime and μ is the minority carrier mobility. Caughey-Thomas [4] data are used for mobility. T is the absolute temperature and k is Boltzmann's constant. These lifetimes become SCAP2D cell parameters used to simulate cell output degradation.

3.3.2 Damage Coefficient Data

Radiation damage is modeled in SCAP2D by reducing the bulk lifetime of the computer constructed cell. But differently doped cells sustain varying

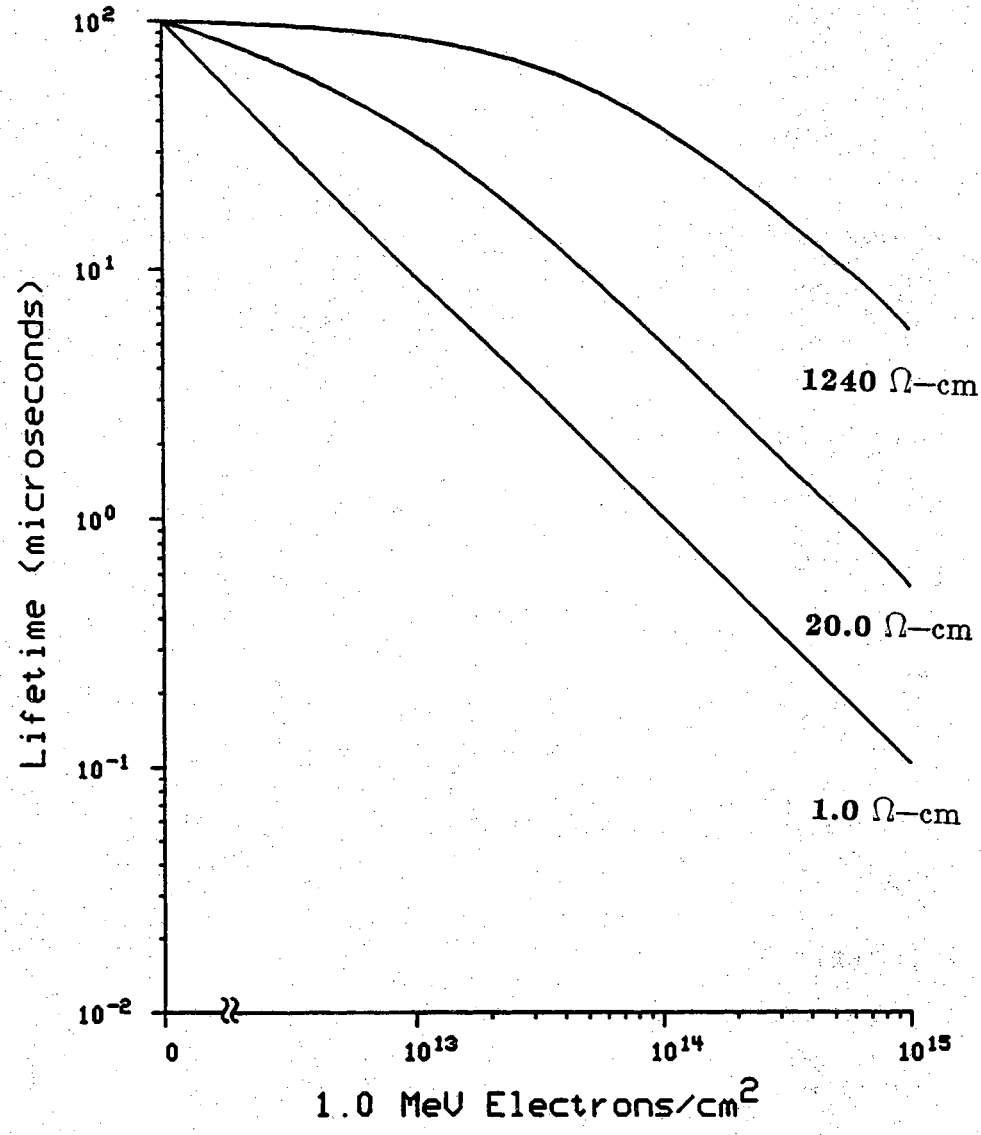

Figure 3.1 1.0, 20., and 1240. Ω—cm cells lifetime degradation as a function of 1.0MeV electrons.

levels of degradation of their respective bulk lifetimes under equal irradiation. This is shown in figure 3.1 that plots lifetime versus 1.0MeV electron fluence for 1.0, 20., and 1240. Ω–cm cells. Therefore, it is preferable to observe the performance of cells versus radiative fluence rather than versus lifetime. For this, laboratory data for $K_l(\rho)$ for 1.0MeV electron equivalent fluence is required.

Damage coefficient data as a function of (boron doped) base resistivity have been assembled from literature. These data assume 1.0MeV equivalent fluence and are appropriate for fluences of order 1.0e15 electrons/cm^2. The data are shown on a composite plot in figure 3.2. The plot shows consistent data from four [5-8] different literature sources. A line is drawn between two of the points to find an empirical formula for the damage coefficient. $K_l(\rho)$ will then be inserted into equation (3.1) to determine the proper diffusion lengths to use as a function of fluence.

Use of equation 3.3 concludes the path taken to model minority carrier lifetime degradation versus incident radiative fluence. First, however, it must be understood what the radiation is doing to the cell, and how the broad spectrum encountered in space is replaced with the equivalent fluence of a monoenergetic particle.

3.4 Equivalent Fluence

3.4.1 The Radiation Spectrum and Damage Equivalence

The high energy particles trapped in the Van Allen belt surrounding the earth include protons, electrons, neutrons, and ions. Each is incident in a

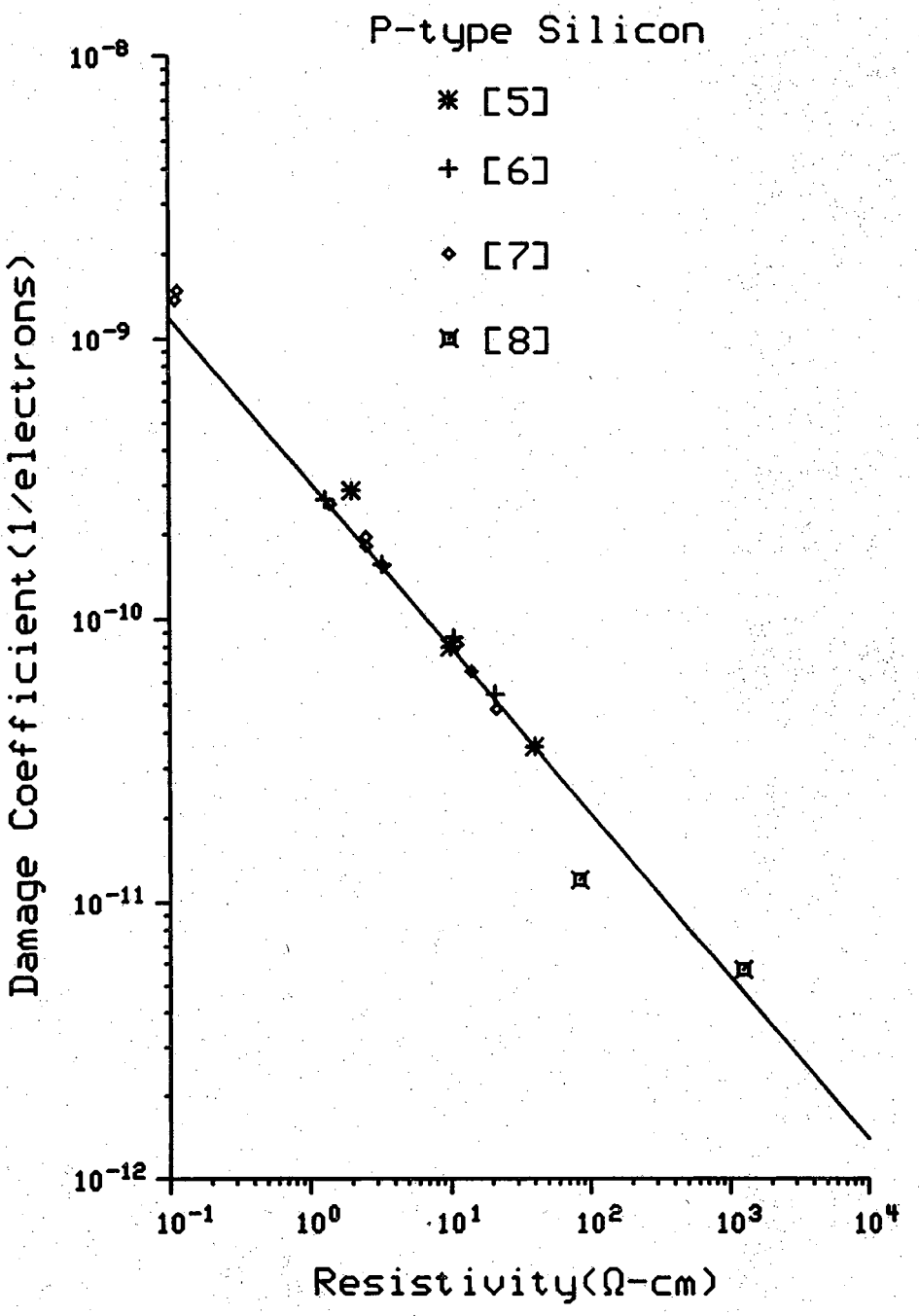

Figure 3.2 Damage coefficient, K_l, versus resistivity. Points represent data from four different sources [5-8]. The line is a linear approximation to the data.

broad spectrum of kinetic energies. The degree of damage to the cell inflicted by an individual particle is clearly going to be a function of the type of particle and its energy. Since this spectrum is too diverse to duplicate in the laboratory, the concept of equivalent fluence is used. Equivalent fluence substitutes the spectrum of particles and energies with a monoenergetic particle normally incident on a specifically shielded solar cell. This substitution is possible because it is the resultant effective minority carrier lifetime that is important to cell performance, not the type of radiation that caused the degradation.

For example, two cells with equivalent effective lifetimes, one a result of 1.0MeV electron irradiation and the other a result of 5.0 MeV proton irradiation, will perform equally well [2]. This is made clear in the following. Damage from incident radiation creates a broad range of trap levels in the energy gap of the semiconductor. The recombination rate is the sum of the recombination rates of each of the individual trap level energies as shown below.

$$R = \sum_{j=1}^{\infty} \frac{pn - n_i^2}{\tau_{n_j}(p + p_j) + \tau_{p_j}(n + n_j)} \tag{3.4}$$

The rate of recombination correlates with an effective lifetime that can be approximated as the result of one trap at the mid-gap.

$$R = \frac{pn - n_i^2}{\tau_n(p + p_i) + \tau_p(n + n_i)} \tag{3.5}$$

Under low injection equation (3.5) reduces further to equation (3.6) for P-type solar cells.

$$R = \frac{\Delta n}{\tau_n} \tag{3.6}$$

SCAP2D cells are modeled with an effective lifetime resulting from a mid-gap energy trap.

3.4.2 Equivalent Fluence of 1.0MeV Electrons

Electrons of energy 1.0MeV are generally employed as an equivalent fluence. This radiation is used because it is easy to produce in a laboratory and the radiation generates relatively uniform damage throughout the cell. The effect of a particle on a cell short circuit current is reflected in equation 3.7 below [6].

$$I_{sc} = I_{sco} - C\log\left[1 + \frac{\Phi}{\Phi_x}\right] \tag{3.7}$$

Φ is irradiative fluence and C is a constant. I_{sc} degradation begins to linearize as a function of the logarithm of fluence near $\Phi=\Phi_x$. Degradation of

I_{sc} (or L_n by equation 3.1) as a result of one particle is compared to the degradation from 1.0MeV electrons. It is then possible to normalize the rate of damage of a different energy particle to that of 1.0MeV electrons. This determines the fluence of 1.0MeV electrons necessary to generate an equivalent amount of damage. For example, to produce the damage done to a solar cell by one 10.0MeV electron requires more than fifteen 1.0MeV electrons [6]. By extending this to all particles incident on the cell, and knowing how many of each particle will be incident on the array for the orbit desired, an equivalent fluence of 1.0MeV electrons can be found to simulate in the laboratory the damage encountered in the space environment.

3.5 Doping Effects on the Damage Coefficient

3.5.1 P-type versus N-type Silicon Damage Rates

Dopants play a large role in how the solar cell withstands irradiation. Proper selection of dopant types (N vs. P), and doping concentrations result in higher end of life efficiencies for the cell although initial efficiencies may not be as high. For example, cells doped P-type are far more tolerant to radiation than N-type cells. We see this in figure 3.3 where the plots of output power show that the P-type is clearly more efficient throughout the lifetime of the cell.

P-type material has a lower K_l than N-type material for equivalent resistivities. The reason for the difference in K_l results from the different damage rates for each dopant type. The calculated displacement rate of 1.0MeV electrons--that is, the rate at which these electrons displace atoms

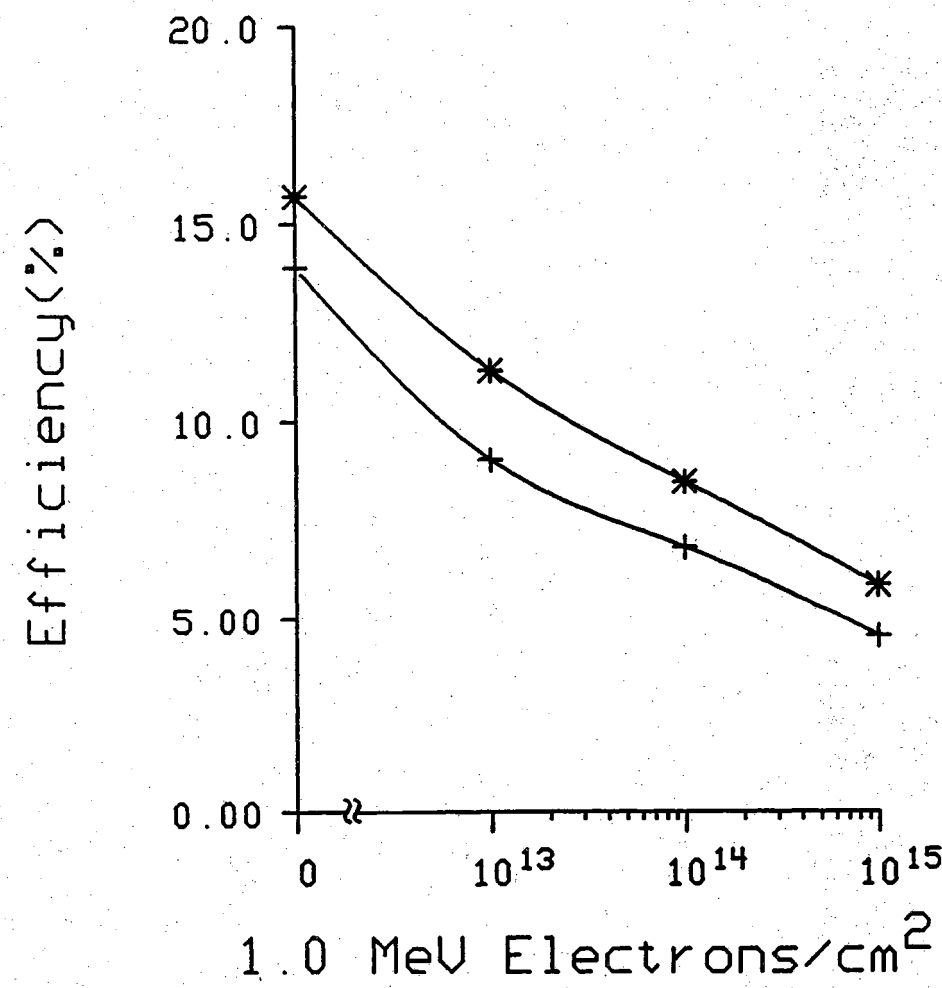

Figure 3.3 P-type and N-type solar cell efficiency as a function of resistivity. N-type damage coefficient taken from Hovel [9].

from their lattice sites--in N-type silicon is 5.2/cm while in P-type silicon it is only 0.03/cm (SCRH p 3-11). Thus, a P-type cell can withstand over 100 times the fluence of 1.0MeV electron radiation that an N-type cell can absorb while sustaining the same amount of damage to the crystal structure. Since lattice displacements lead to recombination centers, it is plain that a P-type cell is better able to maintain its initial lifetime and correspondingly its initial efficiency for a longer period of time.

3.5.2 Effects of P-type Doping Concentration on K_l

Doping concentration also determines the extent of damage to a given solar cell under radiative bombardment. Again, a cell initially higher in efficiency will not necessarily be able to maintain that edge in the hostile space environment. Figure 3.4 plots the efficiencies of two cells with base dopings 1.0 and 20.0. As before with the comparison of N-type and P-type cells, the 20. Ω—cm cell is clearly more efficient than the 1.0 Ω—cm cell. Since the degradation of lifetime varies with changing doping, a model is needed to find appropriate values of lifetime versus doping and radiative fluence.

3.6 Determination of Damage Coefficients versus Resistivity

3.6.1 Introduction

SCAP2D allows simulation of radiation damage by varying the input value of lifetime for a particular cell simulation. But the lifetimes of each cell degrade differently as a function of fluence depending on the resistivity, ρ .

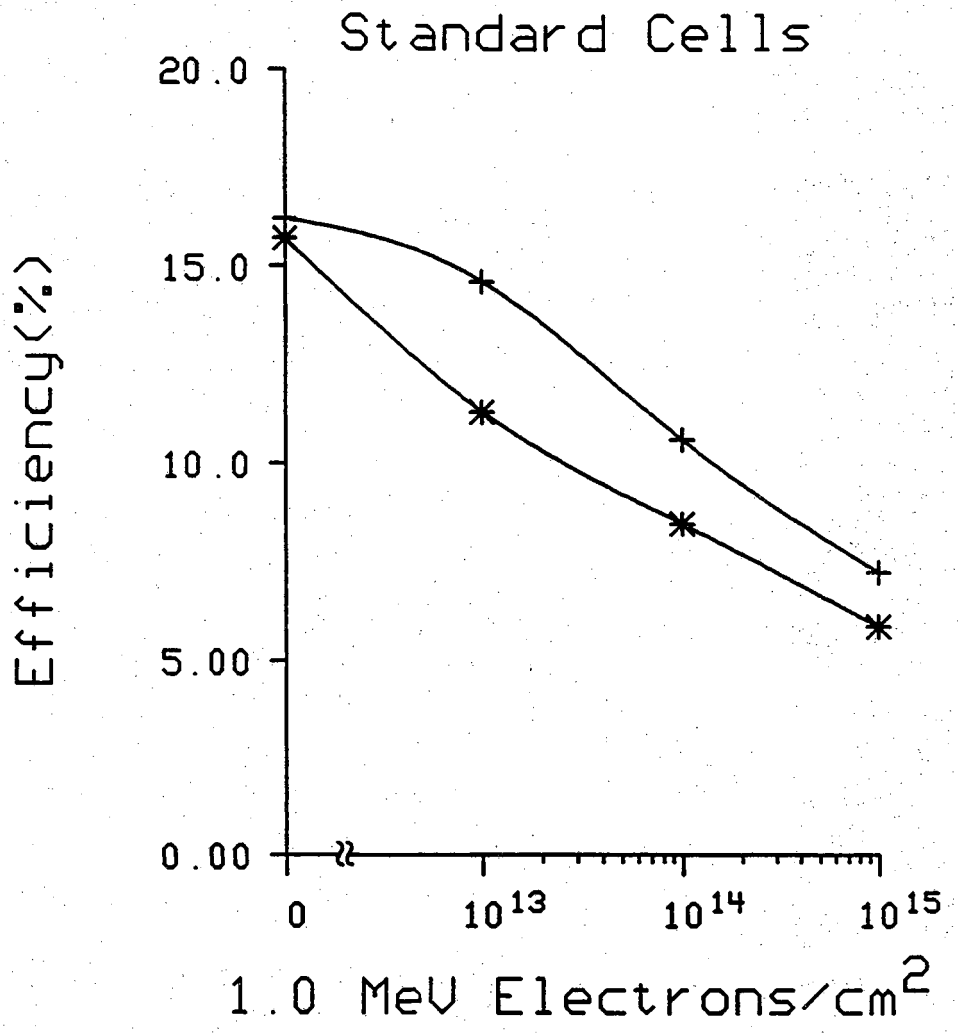

Figure 3.4 Efficiency of P-type standard solar cells with base dopings of 1.0 and 20.0 Ω—cm.

To determine lifetimes after certain fluences of radiation, data is needed for values of $K_\tau(\rho)$. Since lifetime is a difficult parameter to measure experimentally, generally the diffusion length is measured and $K_l(\rho)$, the diffusion length damage coefficient, is calculated from (3.1). Below is a review of one technique for finding $K_l(\rho)$ and an explanation of how the literature data is used.

3.6.2 Laboratory Determination of $K_l(\rho)$

A typical procedure for measuring diffusion length is described by Rosenzweig [10]. A sample solar cell is irradiated with a fluence of 1.0MeV electrons through a thin aluminum shield. If a low enough fluence of electrons is used, it can be assumed that no damage is sustained by the cell during J_{sc} measurements. If the electrons are high enough in energy to assume reasonably uniform electron-hole pair generation within a diffusion length of the P-N junction, the following equation is derived for the short circuit current.

$$J_{sc} = qg_oL_n(1 + \frac{g_1}{g_o}L_n) \tag{3.8}$$

Here, g_o and g_1 are the first two terms in a Taylor series expansion of the generation rate:

$$g(x) = g_o + g_1 x \tag{3.9}$$

Measuring the short circuit current and knowing the generation rate yields the diffusion length. Careful measurement of the diffusion length before and after laboratory irradiation with 1.0MeV electrons yields K_l for the specific cell. However, there are other methods used to find K_l . And it has been shown that K_l is a strong function of incident fluence [11], radiation energy [6], and semiconductor injection level [6]. These variables make finding precise values of K_l versus resistivity difficult.

3.6.3 Finding a Linear Fit to the Laboratory Data

The data points do indicate a possible linear fit, and it has been reported that the slope of the line approximates $\rho^{-\frac{2}{3}}$ [7] for resistivities less than 20 Ω—cm. For the simulations, values for $K_l(\rho)$ given a resistivity are taken from a line drawn through two of the data points. The empirical equation to fit the data is

$$K_l(\rho) = 10.^{[-0.587\log_{10}(\rho)-9.51]} \tag{3.10}$$

Thus, a definite value of $K_l(\rho)$ at each resistivity is known. The values of $K_l(\rho)$ obtained may not be the precise values, but with this $K_l(\rho)$ relation, different resistivity cells can be compared to demonstrate a trend in EOL performance.

Finally, using equation 3.1, diffusion lengths will be found for varying degrees of radiative fluence. Since the value of lifetime is controlled in SCAP2D rather than the diffusion length, lifetimes for each fluence level of 1.0MeV irradiation will be found using equation 3.2.

3.6.4 Independent Degradation of N-type and P-type Regions

Our use of the damage coefficients assumes that the entire cell is P-type. However, the emitter is highly doped N-type, and as such will have a much lower irradiation degraded lifetime than will the comparatively lowly doped, P-type base region. Therefore, the emitter regions must be handled differently. Data for K_l in a highly doped N-type emitter was given by Sater [12]. Thus, τ_p is determined from this K_l and τ_n is found using the $K_l(\rho)$ empirical equation.

Using differing values for τ_n and τ_p does not affect the modeling of cell performance so long as the cell is in low injection. In low injection, the recombination rate is dependent on the minority carrier lifetime as in equation 3.6.

3.7 Modeling Surface Recombination Rates

Since lower energy particles do not penetrate as deeply as the higher energy particles such as our 1.0MeV electrons, the damage from these particles will be confined to regions near the surface of the cell. Thus, there will be a change in the surface recombination with increasing fluence. It is assumed that surface recombination will increase at the same rate that the

bulk recombination of the cell degrades. Therefore, the surface recombination rate is determined by the inverse of the base minority carrier lifetime.

$$S = \frac{C}{\tau_n} \tag{3.11}$$

C is equal to 1.0 centimeter and S is not allowed to exceed 1.0e7 cm/s, the thermal limit. Surface recombination rates are difficult to determine so substantiation of these numbers is unavailable. However, the losses from surface recombination for all cells are so similar that the trend of performance is not significantly affected. Table 3.1 shows the EOL top and bottom surface recombination currents for each type of 20. Ω—cm cell. The current loss from bottom surface recombination (the sun incident side) is nearly the same for each cell at each respective base resistivity. For the top surface recombination current, the tandem junction and EMVJ cells are similar but much larger than the standard cell. The difference comes about as a result of the small region at the top of these two cells where no built-in electric field exists. At EOL especially, this region is highly recombinative and provides significant losses. Even this difference is not of great concern, however, since as was shown in section 2.3.2 that albedo-generated carriers are not collected by the standard cell at EOL. Therefore, there is no real difference in the total losses from surface recombination. Thin standard cells do collect albedo-generated carriers so they incur the smallest surface losses.

Table 3.1 Surface recombination currents for the three cells showing the similar losses suffered from surface recombination.

EOL SURFACE RECOMBINATION CURRENTS (mA/cm^2)						
	Standard		Tandem		EMVJ	
ρ (Ω–cm)	TOP	BOTTOM	TOP	BOTTOM	TOP	BOTTOM
1.0	1.75	3.84	3.54	3.81	4.96	3.87
2.0	1.88	3.76	5.55	3.70	4.92	3.77
10.0	1.84	3.41	5.19	3.35	4.70	3.41
20.0	1.34	3.19	5.16	3.12	4.05	3.19
40.0	1.00	2.90	4.44	2.83	3.67	3.00
84.0	0.71	2.54	2.87	2.47	2.53	2.64
1240	0.86	1.32	1.67	1.33	1.61	1.41

3.8 Conclusions--Incorporation into SCAP2D

We have now found how to reduce the problem of the complex spectrum of space radiation in the Van Allen Belt and its damaging effects on solar cells to a simple equation. Equation 3.1 incorporates a linear fit of $K_l(\rho)$ laboratory data to determine diffusion lengths as a function of base resistivity and 1.0MeV electron equivalent fluence. τ_n and τ_p are found independently by equation 3.1 and are cell parameters in SCAP2D.

Again, the purpose is not to provide precise values for cell efficiency. Rather, SCAP2D will show a trend of how well differently doped cells hold up in the space environment. This will make selection of cell doping and geometry straightforward.

CHAPTER 4

LIMITING FACTORS OF EFFICIENCY OF SOLAR CELLS

4.1 Quantitative Measures of Cell Hardness and Efficiency

The purpose of this chapter is to find the most efficient and radiation hard bilateral solar cells for operation in the harsh space environment. Solar cell radiation hardness is determined by gauging the resistance of a cell to degradation of efficiency as a function of high energy particle fluence. End-of-life (EOL) efficiency and normalized output power are used to quantify this cell performance over time. Normalized output power is found by computing the area under the maximum output power versus 1.0MeV electron/cm^2 fluence curve. (An example of such a plot is shown in figure 1.2) The result is normalized by the total radiative fluence incident at EOL (1.0e15 1.0MeV electrons/cm^2). EOL efficiency measures the "hardness" of a cell to radiation, while the normalized output power combines both initial and final efficiencies to gauge cell performance.

4.2 Limiting Factors of Efficiency--Introduction

The base doping level plays the most significant role in determining the efficiency and radiation hardness of a solar cell. But other factors such as

cell geometry, thickness, and temporary lack of albedo illumination also affect cell performance. In this chapter the limiting factors of cell performance are described using the simulation results.

First, SCAP2D is used to find the base resistivities best able to provide both high initial and high EOL efficiencies for standard P-type cells. It is found that base resistivities between 10.0 and 40.0 Ω—cm show the most promising EOL efficiencies.

Also, different geometries show more promise for sustaining higher efficiencies over the standard solar cell. So the next section studies the performance of the tandem junction and EMVJ solar cells. These geometries improve collection efficiency by introducing collecting junctions at the albedo light incident surfaces. Although the collection efficiency is improved, lower open circuit voltages and lower fill factors limit the improved power efficiencies. The EMVJ cell shows the best performance for most base resistivities.

The standard cell is used in a study of the effect of cell thickness on EOL efficiency. It is found that thinner cells provide higher EOL efficiencies as a result of their higher collection efficiencies over those of the 250. micron standard cells. However, cell fragility can limit the improvement seen. If this limit can be controlled, the improvement in output is significant enough to warrant the use of thinner cells.

Finally, these results are compared to cells without albedo illumination. The thin high resistivity standard cell provides the most power for cells at EOL without the benefits of albedo illumination while the tandem junction is least efficient.

Again, the best solar cell for simultaneously collecting both sunlight and albedo light is the EMVJ cell. However, as the thickness of the standard cell is reduced, it exceeds the EOL efficiency of the EMVJ cell. So which cell is the best? The specific application determines the proper choice for a cell.

4.3 Limiting Factors of Efficiency--Base Doping

4.3.1 Review of Efficiency Data for the Standard Cell

Figures 4.1 and 4.2 show normalized output power and EOL efficiency respectively as a function of base resistivity for P-type standard cells. High and low resistivity cells are less radiation hard than those of the 10-40 Ω–cm range. A different factor is responsible for cell output degradation at each extreme. The reason for the excessive degradation of low resistivity cell output is the higher damage coefficient, K_l. High resistivity cells suffer from a lack of conductivity modulation at EOL.

4.3.2 Accelerated Degradation of Low Resistivity Solar Cell Output

The minority carrier diffusion length, a quantity critical to cell performance, is dependent on the base resistivity in two ways for space-employed solar cells. First, SCAP2D incorporates a relation showing lifetime dependence on doping [13]. This is a pair of empirical formulae that re-compute the lifetime at each node of a simulated cell as a function of total dopants.

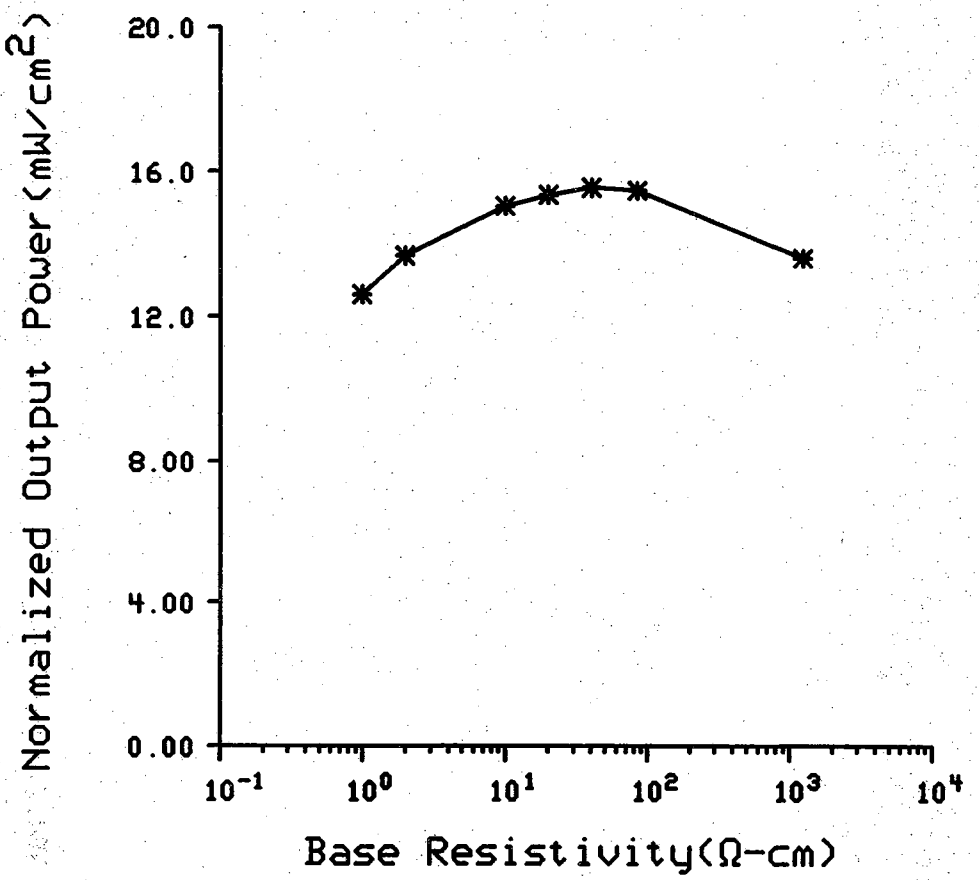

Figure 4.1 Normalized output power vs. resistivity for standard cell.

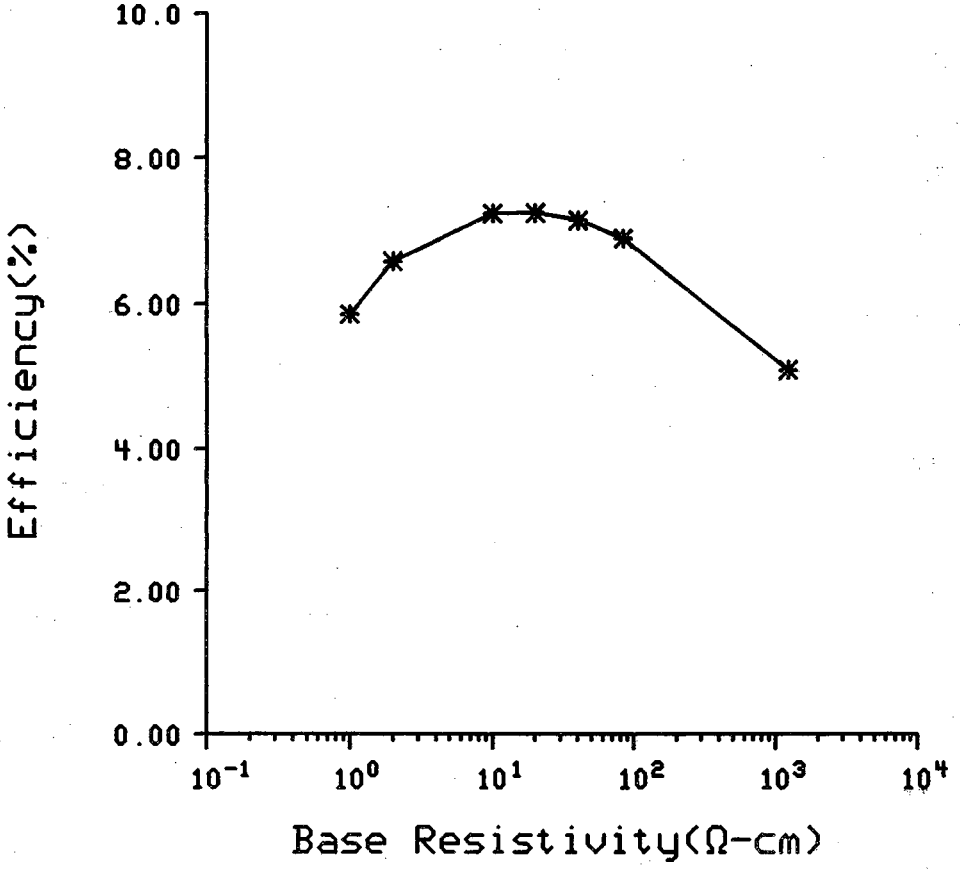

Figure 4.2 End-of-life efficiency vs. resistivity for standard cell.

$$\tau_p = \frac{\tau_{po}}{1 + \frac{N_D + N_A}{N_C}} \tag{4.1}$$

$$\tau_n = \frac{\tau_{no}}{1 + \frac{N_D + N_A}{N_C}} \tag{4.2}$$

τ_{po} and τ_{no} are lifetimes input into SCAP2D. N_D and N_A are the donor and acceptor concentrations respectively. N_C is 7.1e15 cm^{-3}[13]. These equations effectively degrade the minority carrier lifetimes. Second, K_l, is dependent on base resistivity as seen in figure 3.2 so that a highly doped base will suffer more severe diffusion length degradation as a result of irradiation than a lowly doped base.

Thus, cells with low resistivity bases have shorter initial diffusion lengths than do high resistivity cells. A higher damage coefficient amplifies this difference when the harsh space environment further degrades a cell lifetime according to the L_n degradation equation:

$$\frac{1}{L_n^2} = \frac{1}{L_o^2} + K_l(\rho)\Phi \tag{4.3}$$

This is pictured in figure 3.1 where lifetime is plotted versus fluence for three base resistivities (1.0, 20.0, 1240.). With this in mind, one expects that higher resistivity cells would do better as a function of radiative fluence, but

this is only true up to a point. High resistivity cells have lower open circuit voltage and lower fill factor, and the output of these cells degrades because of a lack of conductivity modulation in the base region.

4.3.3 Lower V_{oc} for High Resistivity Cells

Larger reverse saturation current and lack of conductivity modulation combine to limit the performance of high resistivity cells. Higher resistivity bases have wider depletion regions on the base side of the emitter-base junction. Therefore, a larger reverse saturation current, J_o, exists given as:

$$J_o = q\left[\frac{D_N}{L_N}\frac{n_i^2}{N_A} + \frac{D_P}{L_P}\frac{n_i^2}{N_D}\right] \tag{4.4}$$

Since emitter doping is always much greater than the base doping, $N_D \gg N_A$ so that J_o is inversely proportional to the base doping.

$$J_o = q\frac{D_N}{L_N}\frac{n_i^2}{N_A} \tag{4.5}$$

Looking at equation 4.6 for V_{oc}, the open circuit voltage is inversely proportional to the natural log of J_o.

$$V_{oc} = \frac{kt}{q} \ln \left[\frac{J_{sc}}{J_o} + 1 \right] \tag{4.6}$$

These equations show that lower base doping leads to smaller open circuit voltages.

4.3.4 Lack of Conductivity Modulation in High Resistivity Cells

Lack of conductivity modulation is discused by Schwartz[14] et. al. as a problem associated with concentrator cells. There, high current conditions deplete the excess carriers from the back of the high resistivity cell. This creates a region of low conductivity increasing the voltage drop across the base region of the photodiode. An explanation of the degrading effect of lack of conductivity modulation for space applications was described by Weinberg et. al. [15] and is aided by an equivalent circuit of the photo diode shown in figure 4.3.

The current source represents current from light-generated carriers. The diode, when forward biased, produces the dark current, or recombination current, by injecting minority carriers into the base and emitter regions where they recombine. Therefore, larger V_D and larger J_o produce a larger recombination current as seen in equation 4.7.

$$J_{dark} = J_o(e^{\frac{qV_D}{kT}} - 1) \tag{4.7}$$

V_D is largest under open circuit conditions when all the current is

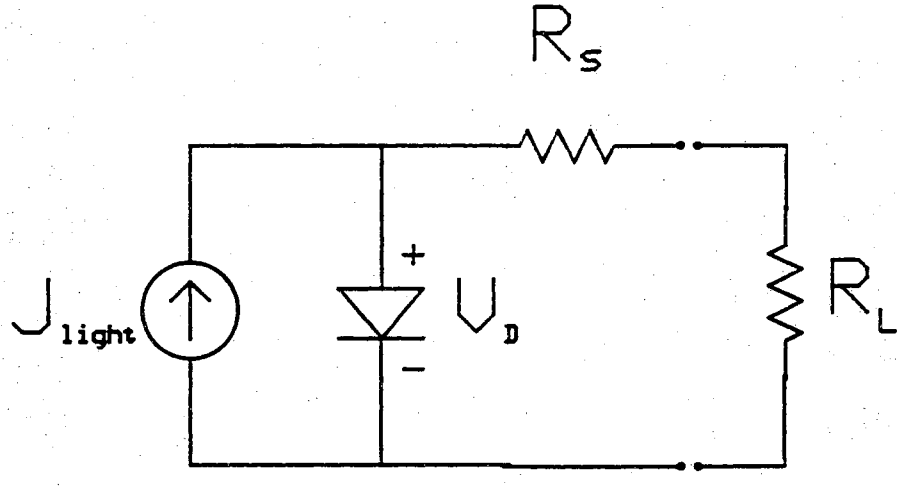

Figure 4.3 Equivalent circuit of a photodiode.

recombination current. R_s is the series resistance encountered in the base of the diode and the contact lines. Neglecting contact resistance, R_s will depend on the carrier concentration in the base as follows:

$$R_s = \int_0^{L_B} \frac{dy}{q(\mu_n(y)n(y) + \mu_p(y)p(y))} \tag{4.8}$$

where L_B is the length of the base and R_s has units $\frac{\Omega}{cm^2}$.

Under illumination, photo-generated hole-electron pairs increase the base carrier concentration. High injection in high resistivity solar cells enhances the conductivity of the base. This conductivity modulation reduces R_s so that the cell operates more efficiently. But radiation introduces recombination centers throughout the cell reducing the excess carrier concentration and accordingly, the conductivity. Now, there is a LACK of conductivity modulation, and R_s becomes a factor in cell performance.

Referring back to figure 4.3 and setting R_l =0.0 (short circuit condition), the voltage drop across the base is also the voltage drop across the diode. The recombination current is the dark current of a biased diode given by equation 4.7.

Remembering that J_o is larger with a higher resistivity cell, the dark current produced by this cell is larger than for a lower resistivity cell. Also, larger $V_B = V_D$ results in more carriers being injected into the base and emitter regions where they become minority carriers. These carriers

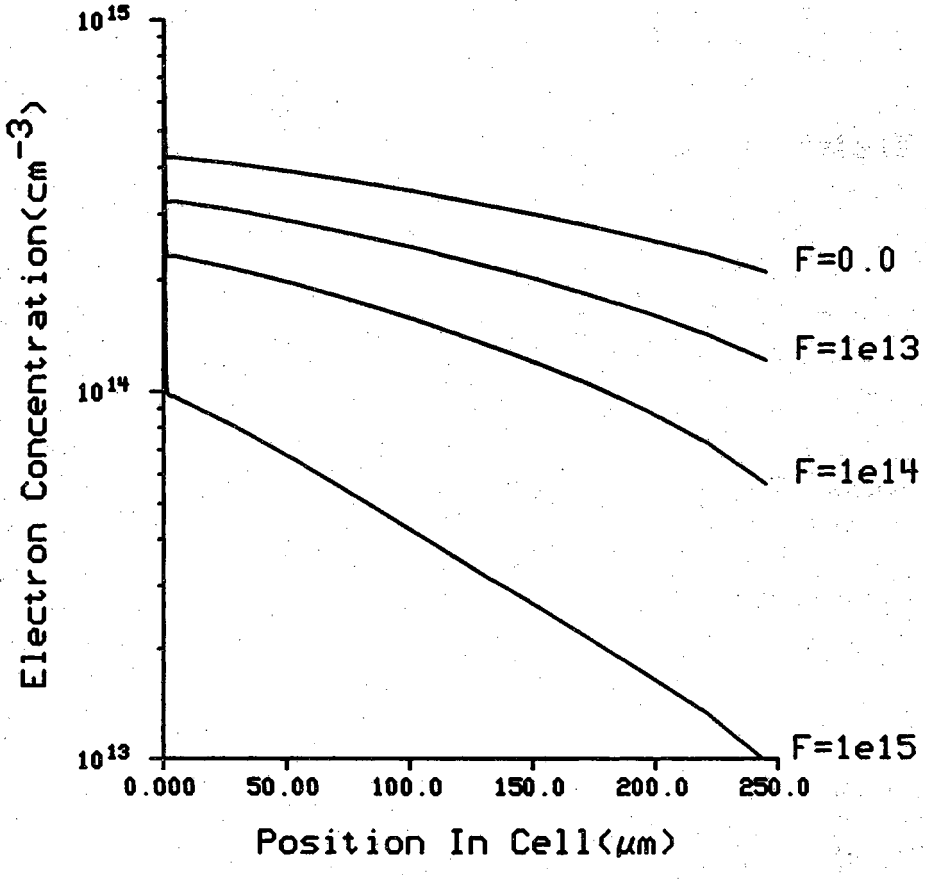

Figure 4.4 Electron Concentration at maximum power for 1240 Ω–cm cell for four different levels of 1.0MeV electron fluence.

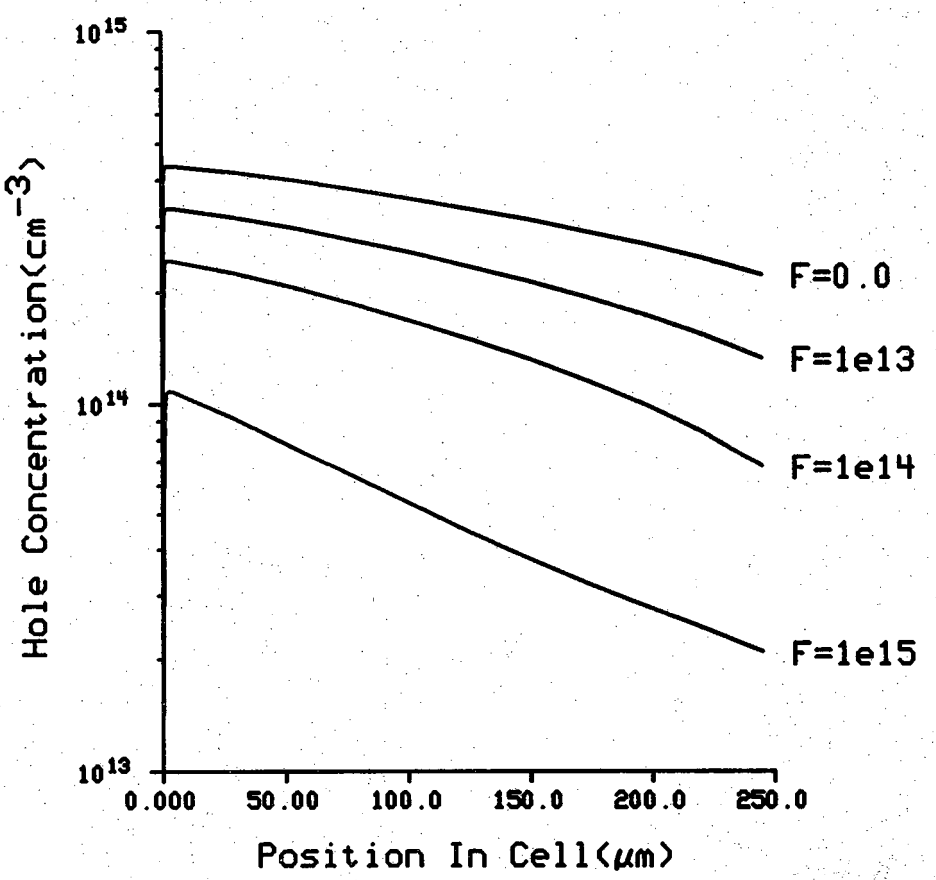

Figure 4.5 Hole Concentration at maximum power for 1240 Ω—cm cell for four different levels of 1.0MeV electron fluence.

recombine so that the result is a smaller J_{sc}. Figures 4.4 and 4.5 show hole and electron concentrations at P_{max} for increasing radiative fluence. These concentrations are for a line under the contact about 2.0 microns from the left side of the unit cell. The concentrations drop by an order of magnitude from initial to EOL concentrations so that R_s increases accordingly. J_{mp} of the 1240 Ω—cm standard cell is reduced from 54.2 to 27.6 milliamperes so that V_B, the voltage drop across the base, will increase about five times. This loss manifests itself as a reduction in the fill factor.

4.3.5 Degradation of Fill Factor

Figures 4.6 and 4.7 are J-V plots of a 1240. Ω—cm cell and a 10.0 Ω—cm cell. These plots show the degradation of fill factor for the 1240. Ω—cm standard cells as a loss of "squareness" of the J-V curve. The 10.0 Ω—cm cells retain the square shape for all levels of fluence while the 1240. Ω—cm cell becomes somewhat triangular. High injection is never reached in 10.0 Ω—cm cells under one sun illumination since the base is highly doped. As a result, R_s is not a factor and conductivity modulation is not necessary for efficient operation. But in lowly doped cells, conductivity modulation enhances the performance of the cell by preventing a large voltage drop from appearing across the base region.

4.4 Limiting Factors of Efficiency--Contact and Doping Geometry

Chapter 2 introduced the tandem junction and EMVJ solar cells as promising geometries capable of collecting albedo-generated carriers even

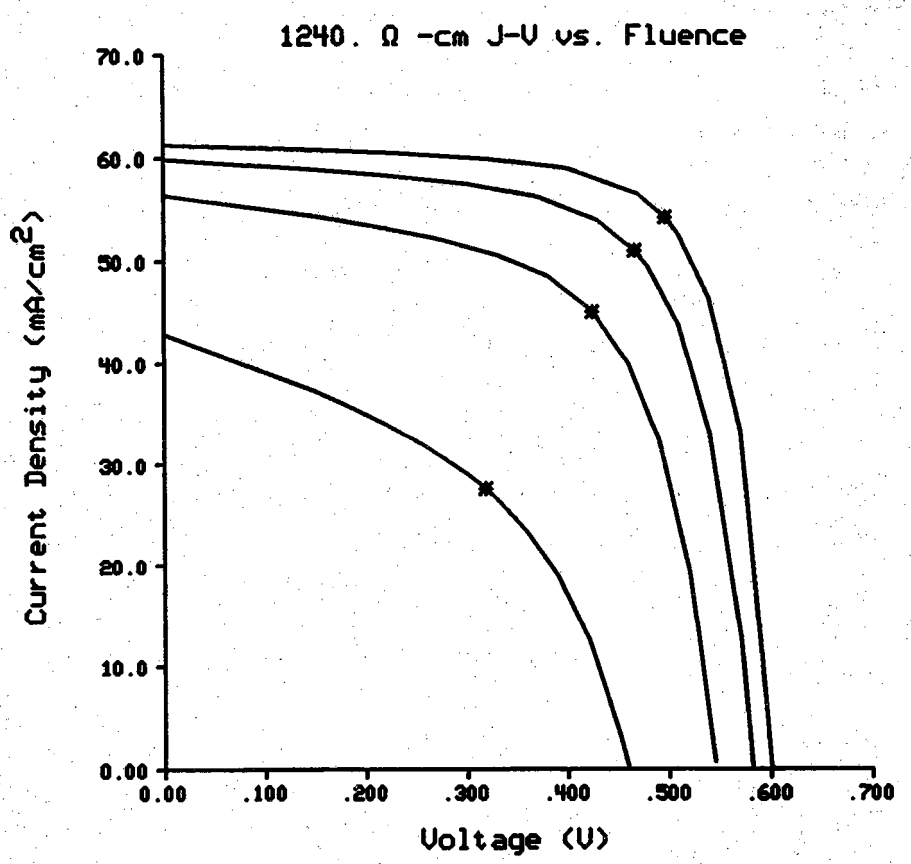

Figure 4.6 J-V plot of 1240. Ω–cm standard cell. Stars mark maximum power points.

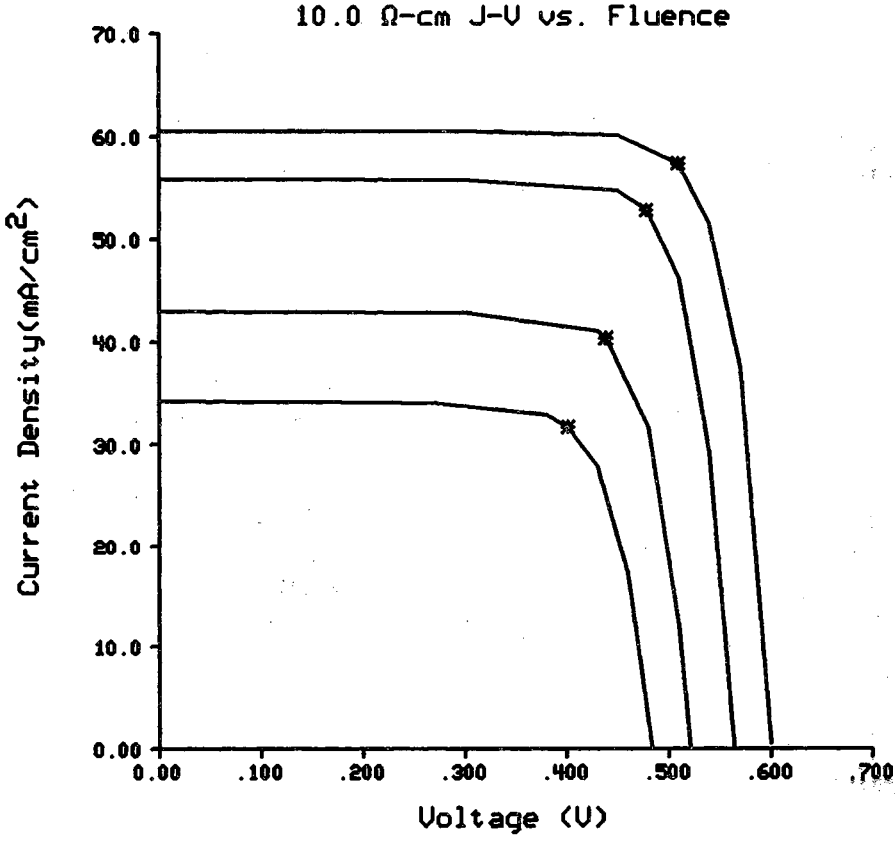

Figure 4.7 J-V plot of 10. Ω—cm standard cell. Stars mark maximum power points.

under low lifetime conditions. Higher EOL efficiencies are expected with these geometries. It is found that the EMVJ cell is the most radiation hard of the three geometries while the standard cell is the weakest. Both the alternative geometries improve short circuit current over the standard cell at EOL, but improvement in the output power is limited by lower open circuit voltages and fill factors inherent with the alternative cell geometries. In this section the factors limiting the EOL efficiency of each cell are investigated.

Figures 4.8 and 4.9 show normalized output power and EOL efficiencies for each of the three cell geometries. The EMVJ cell delivers the most power of the three cells while the standard cell, with little or no albedo collection at EOL, provides the least. The output power of each cell peaks near a base resistivity of 20.0 Ω—cm. The normalized output power and EOL efficiency plots show the same peaks and basic curves versus resistivity. This shows that EOL efficiency is the dominant factor in determining the normalized output power of a cell. Thus, the initial efficiency is less important than the final efficiency in gauging solar cell performance in space applications.

Tables 4.1-4.3 list EOL parameters for all cell types and resistivities. From these tables the limits on efficiency for each cell can be isolated. At EOL the standard cell has the highest V_{oc} , but provides the least current of the three cells. These results occur because the standard cell doesn't have a collecting junction at the albedo surface. J_{sc} increases with the tandem junction cell over the standard cell. This increase results from the added collecting junction at the albedo surface. Carrier collection is further improved with the EMVJ cell as a result of the 100. micron etched contacts

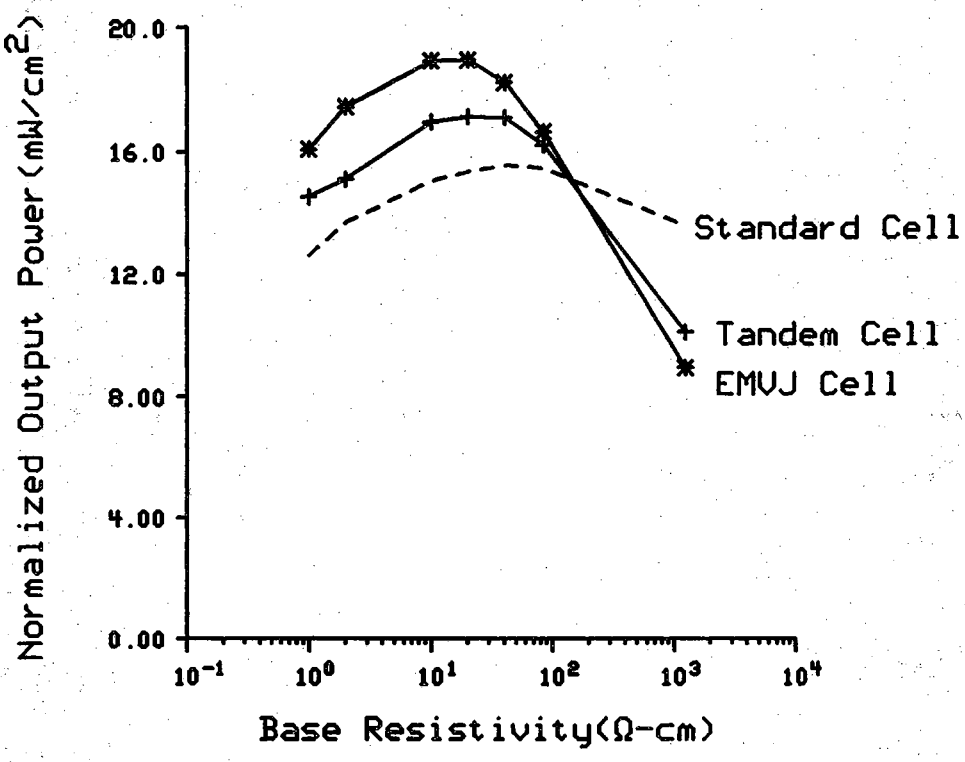

Figure 4.8 Normalized output power versus resistivity for standard, tandem junction, and EMVJ cells.

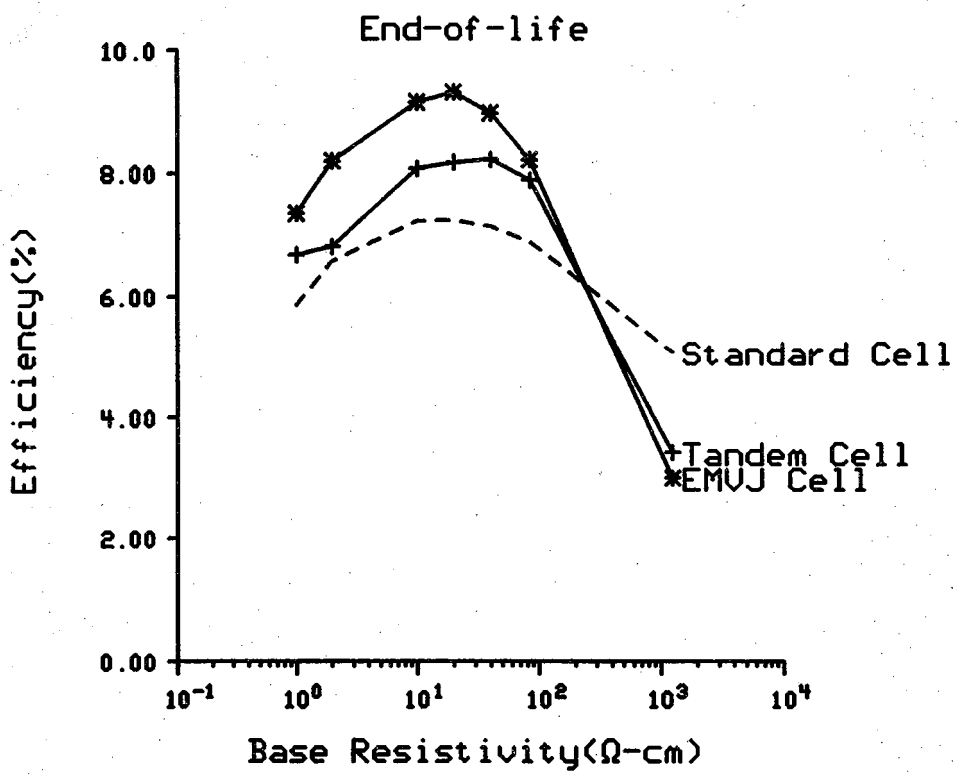

Figure 4.9 End-of-life efficiency versus resistivity for standard, tandem junction, and EMVJ cells.

Table 4.1 Standard cell parameters.

EOL STANDARD SOLAR CELL PARAMETERS				
ρ (Ω–cm)	V_{oc} (V)	J_{sc} (mA)	F.F.	Eff(%)
1.0	0.497	27.1	0.767	5.86
2.0	0.496	30.0	0.776	6.58
10.0	0.483	34.2	0.769	7.23
20.0	0.474	35.7	0.753	7.24
40.0	0.464	37.5	0.722	7.14
84.0	0.453	40.4	0.662	6.89
1240	0.460	42.9	0.445	4.98

Table 4.2 Tandem junction cell parameters.

EOL TANDEM JUNCTION SOLAR CELL PARAMETERS				
ρ (Ω–cm)	V_{oc} (V)	J_{sc} (mA)	F.F.	Eff(%)
1.0	0.464	34.9	0.726	6.68
2.0	0.447	38.9	0.689	6.81
10.0	0.442	44.8	0.717	8.08
20.0	0.432	46.9	0.710	8.18
40.0	0.421	48.9	0.702	8.23
84.0	0.408	51.3	0.663	7.89
1240	0.397	32.8	0.462	3.42

Table 4.3 EMVJ solar cell parameters.

EOL EMVJ SOLAR CELL PARAMETERS				
ρ (Ω–cm)	V_{oc} (V)	J_{sc} (mA)	F.F.	Eff(%)
1.0	0.443	42.3	0.691	7.35
2.0	0.446	45.6	0.709	8.20
10.0	0.436	51.4	0.719	9.16
20.0	0.426	53.1	0.724	9.32
40.0	0.412	54.6	0.702	8.98
84.0	0.403	56.4	0.636	8.22
1240	0.392	30.1	0.422	3.10

that collect carriers deep in the cell that would otherwise recombine. An additional advantage results from reduced shadowing on the front surface of the EMVJ. However, the increased N+P junction area from the additional collecting junctions on both cells lowers V_{oc} and the fill factor. The tandem junction cell has more emitter junction area than the standard cell and so it has a smaller V_{oc}. The EMVJ cell has even more emitter area so V_{oc} is further reduced. The EMVJ cell has the highest J_{sc}, but the lowest V_{oc} and a low fill factor. The tandem junction cell has the lowest fill factor for most resistivities.

Despite these limits, the EMVJ cell is the most efficient at EOL. This is true even though the tandem junction cell has a higher initial efficiency. The EMVJ also provides the most power during a given mission as shown by the normalized output power plots of figure 4.8. The standard cell has the highest EOL V_{oc} and fill factor but is the least efficient of the three cells at EOL.

4.5 Limiting Factors of Efficiency--Cell Thickness

Thinner standard cells can collect albedo-generated carriers at EOL. Figure 4.10 shows output power versus thickness for the 20.0 Ω–cm standard cell. The 50.0 micron cell produces about 27% more power than the 250. micron thick cell. This improvement comes about from the reduced distance albedo-generated carriers must diffuse before reaching the collecting junction.

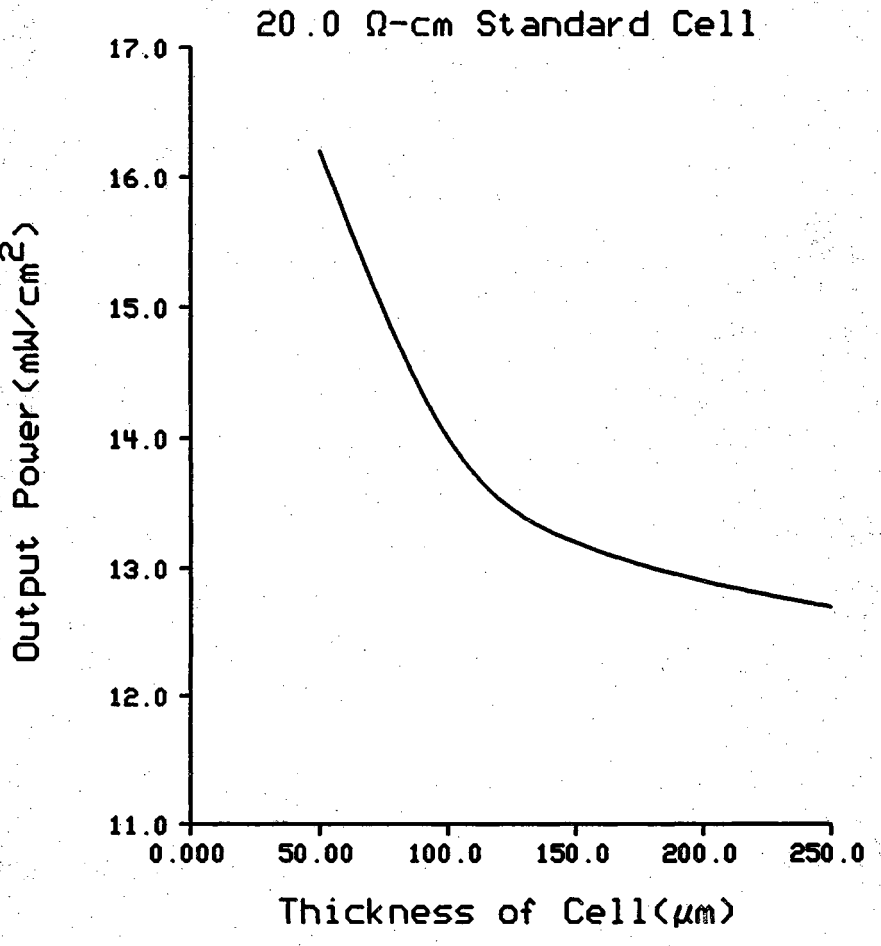

Figure 4.10 End-of-life maximum output power versus cell thickness.

Note the increasing slope of EOL efficiency versus thickness in figure 4.10. The generation rate increases exponentially nearer the surface. So as the cell thickness is reduced, the output power increases rapidly as increasingly more albedo-generated carriers are created within a diffusion length of the collecting junction. The diffusion length at EOL for a 20.0 Ω—cm cell is approximately 40. microns. Only a 4.% improvement is seen for 20.0 Ω—cm, thinner tandem junction cells. The tandem junction cell has an additional emitter so that albedo carriers are collected at the back surface, not the front. Thus, no benefit at EOL is found by reducing the thickness. No simulations of thin EMVJ cells were done since etching weakens the cell structurally. The etched contacts would further weaken the flimsy thin cell.

Table 4.4 lists EOL output power for 250. and 50. microns cells of all resistivities. The percent gain is also listed. The tremendous gain seen for the higher resistivity cells is a result of overcoming the lack of conductivity modulation. Equation 4.8 shows that a shorter base length reduces the series resistance. The shorter base also increases the average excess carrier concentration. Figure 4.11 compares the electron concentrations for the 250. and 50. micron cells. While the local electron concentration is lower, the low carrier concentration base region is much shorter than that of the 250. micron cell. Lower R_s results in a higher fill factor.

The 1240. Ω—cm cell represents the highest resistivity base used for the solar cells modeled in this work. It is the most efficient cell of the 50. micron cells modeled while it was the least efficient of the 250. micron cells. This suggests that increasing the resistivity further will lead to higher efficiency

Table 4.4 End-of-life output power for 250. micron and 50. micron standard cells with percent gain.

250. and 50. MICRON STANDARD CELL EOL OUTPUT POWER			
ρ (Ω–cm)	250. μm($\frac{\text{mW}}{\text{cm}^2}$)	50. μm($\frac{\text{mW}}{\text{cm}^2}$)	Gain(%)
1.0	10.3	10.4	0.97
2.0	11.6	12.0	3.45
10.0	12.7	15.1	18.9
20.0	12.7	16.2	27.6
40.0	12.6	16.9	34.1
84.0	12.1	17.4	43.8
1240.	8.76	18.5	111.

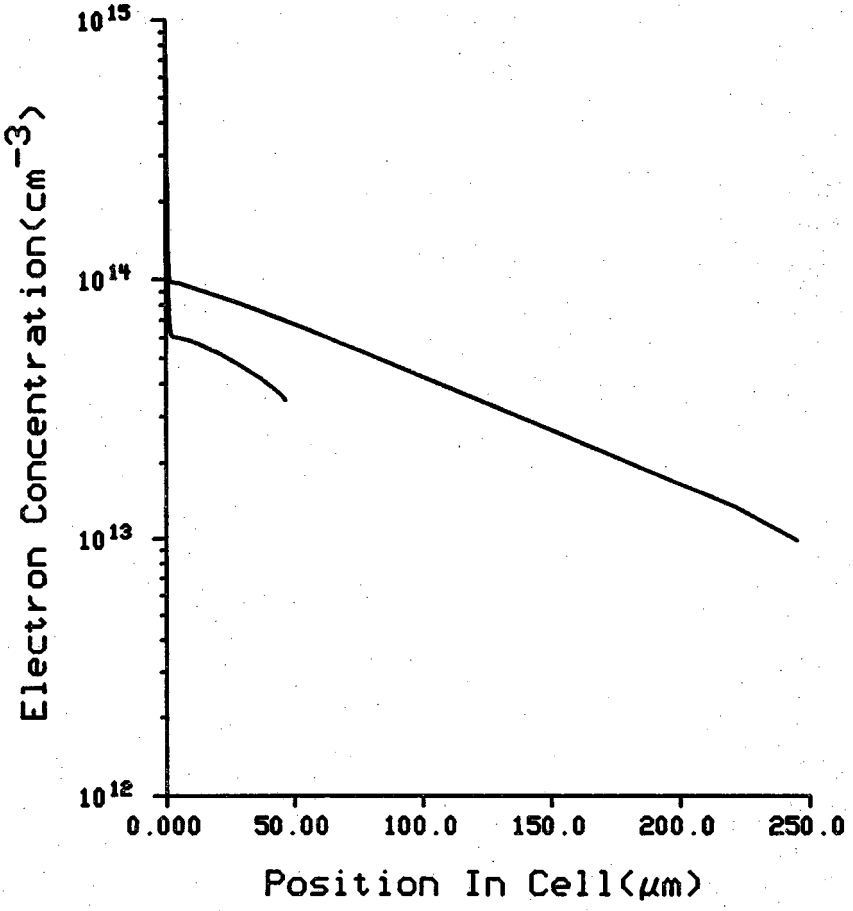

Figure 4.11 Electron concentrations for 250. and 50. micron 1240. Ω—cm standard cells at end-of-life and maximum power.

cells. Higher resistivity, thinner solar cells are the most efficient solar cells when trying to collect both front illumination and albedo illumination at EOL.

Possible gain in output power by use of thinner cells is limited by their fragility. Significant improvement in the 20. Ω—cm thin standard cell efficiency begins at a thickness around 100. to 150. microns. At this point the cells are so thin that they are more likely to break during a mission. The damaging effect of one broken cell is multiplied by the number of cells in its respective series. So one broken cell can significantly reduce the output power of the array. Thin cells display significant advantages in power to weight ratio, but their fragility must be accounted for when considering them for use in space missions.

4.6 Limiting Factors of Efficiency--Albedo Turned Off

4.6.1 Introduction

Additional collecting junctions at the albedo surface improve carrier collection for the tandem junction and EMVJ solar cells. But how do these improvements to the standard cell affect cell performance when the albedo is dark? The EMVJ cell is the best collector of albedo carriers, a quality that is critical at EOL. However, during much of the orbit time, there is no albedo illumination. It has been shown that the additional collecting junctions force lower V_{oc} and fill factor. Therefore the standard cell is expected to be the most efficient under dark albedo conditions.

In this section, the performances of the cells without albedo illumination are compared. Three significant findings are observed. First, the standard cell is the most efficient cell without albedo illumination. Also, the thin high resistivity standard cell outperforms the 250. micron standard cell. Second, the benefit from the presence of albedo carriers is twofold. These carriers not only improve the output power by their collection, but also aid the collection of front generated carriers by enhancing the conductivity at the back of high resistivity cells. Finally, the EMVJ cell is comparable in efficiency to the standard cell under these conditions. Therefore, since the intensity of albedo light varies from 30.% of one-sun intensity to 0.%, the EMVJ cell will provide the most power of the 250. micron cells during an orbit.

4.6.2 J_{sc} Comparisons With and Without Albedo Light

Figure 4.12 shows EOL efficiencies for all cells and base resistivities. As stated, the standard cell is the most efficient of the 250. micron cells although the EMVJ cell is comparable in performance. All 250. micron cells peak around 20. Ω–cm as they did with albedo illumination. The 84. Ω–cm thin cell is the most efficient of all.

Table 4.5 lists J_{sc} for standard cells at EOL with and without albedo illumination. The data show that little collection of albedo carriers is present even for the higher resistivity cells. This is, of course, because of L_n degradation. Little difference exists in J_{sc} with and without albedo illumination for all standard cells except the 1240. Ω–cm cell. The large

difference seen for the 1240. Ω–cm cell with and without albedo light results from a more severe lack of conductivity modulation in the cell when albedo light is incident. The lack of improvement in J_{sc} for 250. micron standard cells with albedo light over those without albedo light incident shows the ineffectiveness of the BSF as a minority carrier reflector at EOL.

4.6.3 Ineffectiveness of Back Surface Field at EOL

The loss of albedo collection shows the ineffectiveness of the BSF as a minority carrier reflector in low lifetime standard cells. SCAP2D calculates recombination totals in each region of the modeled cell. In table 4.6 are recombination data at EOL for a 20. Ω–cm cell identical to that pictured in figure 1.1. This cell is then modeled without a BSF. Table 4.6 shows that a BSF does not enhance the collection efficiency of the cell at this low lifetime. The BSF simply changes the recombination percentages. For the cell without the BSF, the percentage of the total recombination at the surface is higher than the cell with a P+P junction. But the base recombination is correspondingly lower so that the total recombination current has not changed. It is the minority carrier diffusion length that controls the effectiveness of the BSF.

The base minority carrier diffusion length at EOL is 40. microns and is much shorter than the thickness of the 250. micron device. The BSF sweeps the photo-generated electrons from the highly recombinative surface to the base region. Here, the electrons are still minority carriers. Once radiation reduces the bulk minority carrier lifetime to a low enough level, the carriers are further than a diffusion length from the collecting junction. These

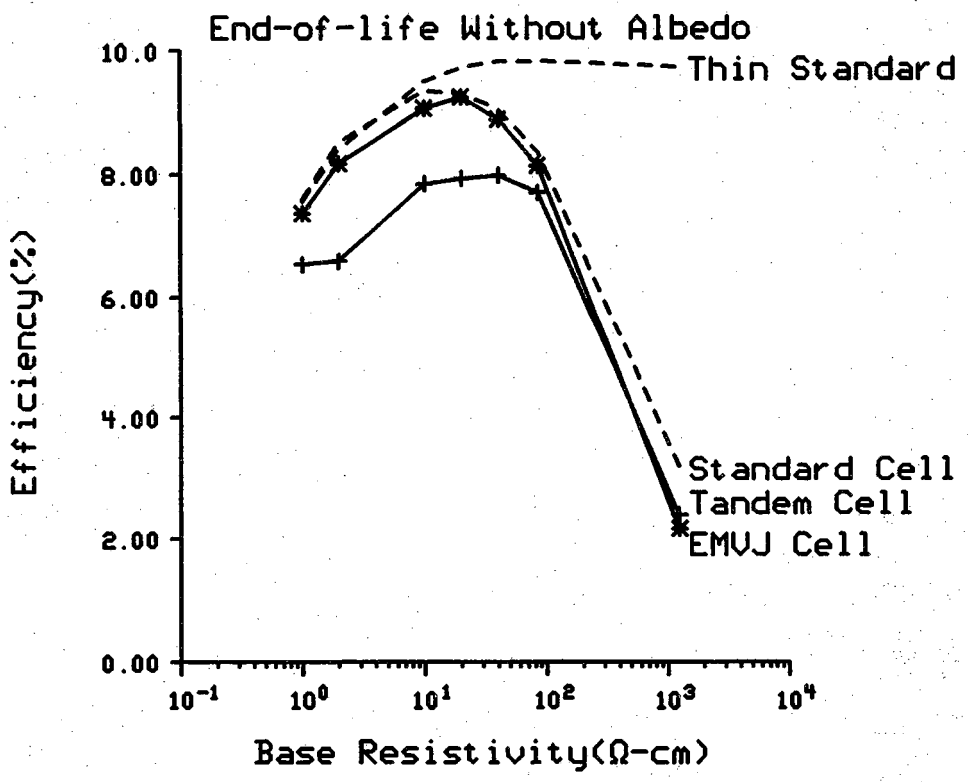

Figure 4.12 End-of-life efficiencies without albedo illumination.

Table 4.5 Short circuit current with and without albedo illumination.

250. MICRON STANDARD CELL EOL J_{sc}			
ρ (Ω–cm)	With Albedo J_{sc}(mA)	Without Albedo J_{sc}(mA)	Gain(%)
1.0	27.1	27.0	0.37
2.0	30.0	29.9	0.33
10.0	34.2	34.1	0.29
20.0	35.7	35.4	0.85
40.0	37.5	36.9	1.63
84.0	40.4	38.6	4.66
1240.	42.9	26.6	61.3

Table 4.6 Regional recombination currents in P-type standard cell.

MAXIMUM POWER RECOMBINATION CURRENTS					
Cell	η_c	BSF Surface	Base	N+	Total
NO BSF	56.8	13.0	11.8	1.63	30.1
BSF	56.6	1.34	23.7	1.62	30.0

carriers won't be collected. At EOL the BSF only changes the region in which the carriers recombine. Electrons are swept away from the surface, but recombine in the base. Therefore, the P+ regions should be designed to make the best contact possible and shouldn't be thought of as minority carrier reflectors. The BSF is, however, important for thinner standard cells.

4.6.4 Albedo Light Aids Collection of Front-generated Carriers

Albedo light generates additional hole-electron pairs improving the output power of a solar cell. Because most of the carriers are generated near the back of the cell, albedo-generated carriers also assist in the collection of front-generated carriers by increasing the conductivity at the back of the cell. If no albedo light is present, two factors reduce the excess carrier concentration in the cell. First, as the diffusion length degrades with fluence, fewer excess carriers can diffuse to the back of the cell. The excess

carrier concentration is lowered throughout the cell, but it is most severe at the back of the cell.

Second, under high current conditions, more excess carriers are extracted from the back of the cell near the BSF junction. This lowers the local excess carrier concentration at the back of the cell even further. This is depicted in figure 4.13 where lower voltage values lead to lower carrier concentrations. Thus, R_s increases with current so that a cell suffers more severely from a lack of conductivity modulation under high current conditions. Albedo illumination alleviates this problem by generating carriers near the back surface. It is a source of carriers that prevents the back region from becoming overly depleted under high current conditions. Figures 4.13 and 4.14 show the electron concentration for a 1240. Ω–cm cell for varying voltages with and without albedo illumination respectively. They show that most of the base region has fewer excess carriers without albedo illumination and that the difference is most drastic near the BSF junction.

4.7 Additional Output Power From Albedo Light

Tables 4.7-4.10 show improvement in EOL output power from albedo illumination for all the cells modeled. Each cell is compared to the standard, bilateral cell without albedo illumination and the percent improvement in output power is also listed. All cells show some improvement except the 250. micron standard cell. The best cells are the thin standard cells and the EMVJ cells. The tandem junction cell shows some improvement, but not enough to merit use because the full albedo

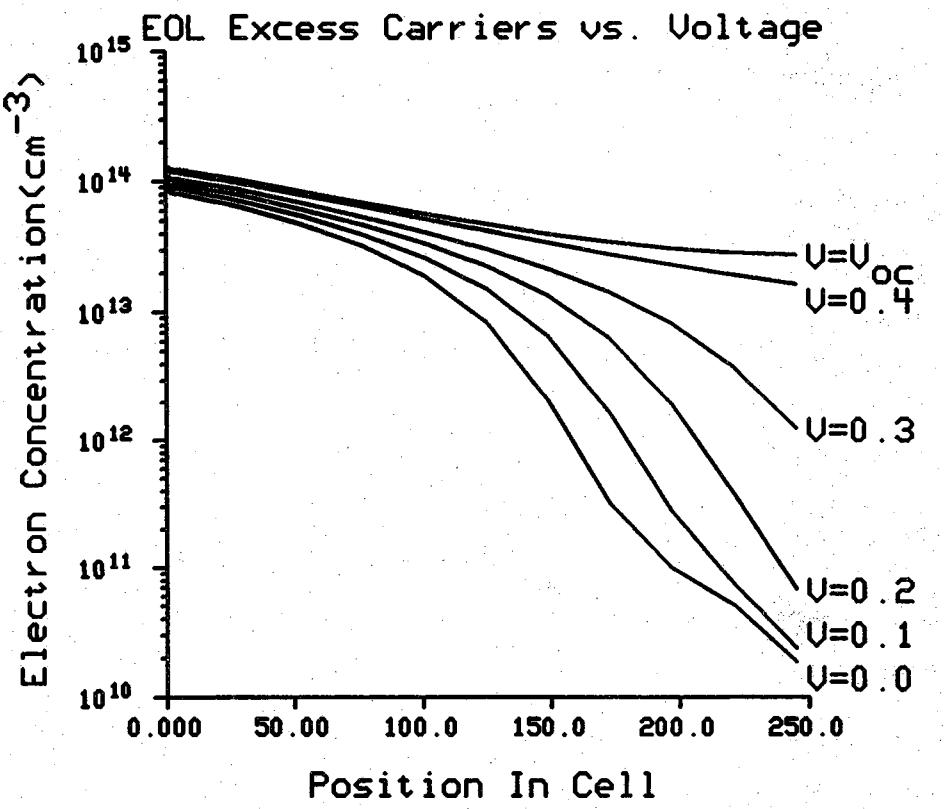

Figure 4.13 Electron concentrations versus position in cell for varying voltages without albedo.

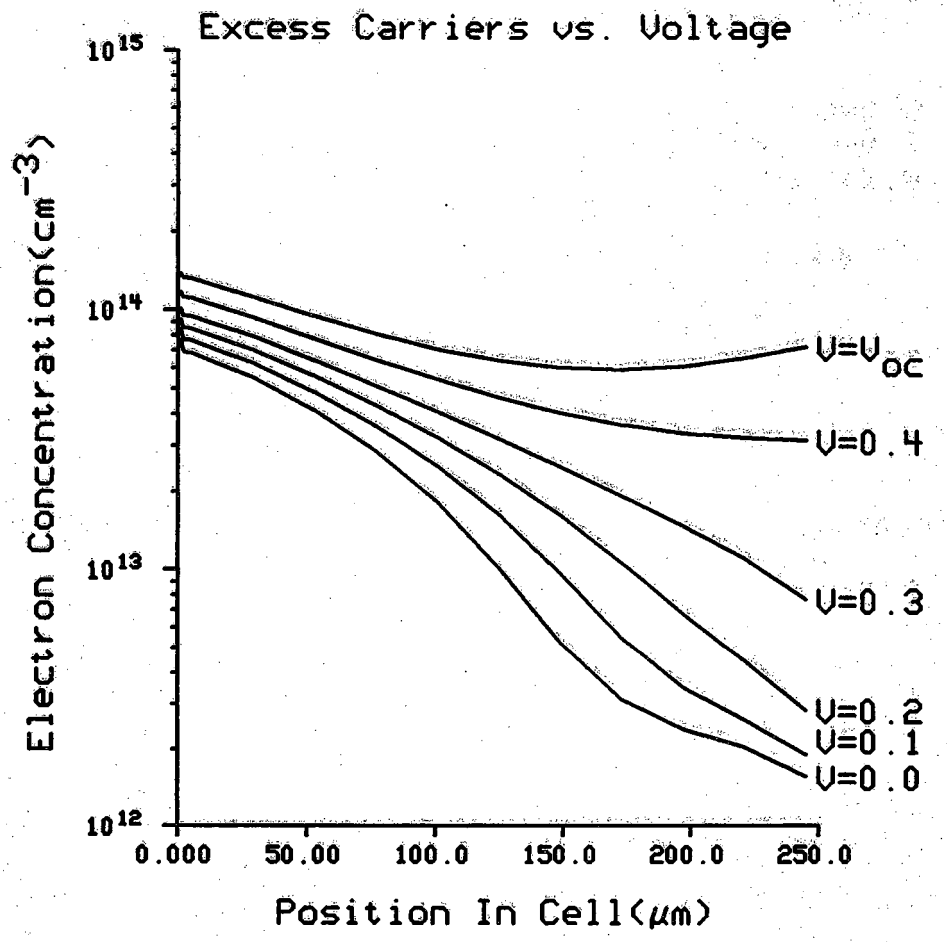

Figure 4.14 Electron concentrations versus position in cell for varying voltages with albedo.

intensity is only present for a short period of time as seen in figure 2.1. The tandem junction cell is less efficient than the 250. standard cell when the albedo is dark, and the albedo is present less than half the time. Therefore, the gain with albedo is negated by the loss in power without albedo.

The cells with the most promise are thin standard cells. These cells show marked improvement in EOL output power and are simpler to process over the etched cell. If cell breakage can be eliminated, significant gain in output power can be realized from albedo light without loss in output power from one sun incidence.

4.8 Limiting Factors of Efficiency--Conclusions

The best cell to use for collection of albedo-generated carriers at EOL depends on the limiting factors of the application. For instance, for the 250. micron cells the EMVJ cell provides the most EOL power at full albedo intensity and is comparable to the standard cell when no albedo light is incident. However, the additional processing steps necessary during EMVJ fabrication make the cell more expensive to produce. Also, the etched contact weakens the cell physically so that it may also suffer from breakage.

The thin high resistivity standard cell supplies the most power from sunlight alone. Also, thinner standard cells produce more power than the EMVJ cell when albedo light is incident on the back, so that the thin standard cell can provide a cheaper alternative to the EMVJ cell. Both the EMVJ and the thin standard cell are limited by their fragility. The tandem junction shows limited improvement in EOL with albedo incidence, and less

one-sun output power at EOL. The loss in one-sun collection over the 250. standard cell makes the tandem junction cell less desirable than the others.

Table 4.7 Standard 250. micron cells at EOL showing improvement with albedo illumination.

STANDARD CELL EOL OUTPUT POWER			
ρ (Ω–cm)	Standard Cell Without Albedo($\frac{mW}{cm^2}$)	Standard Cell With Albedo($\frac{mW}{cm^2}$)	Percent Gain(%)
1.0	10.3	10.3	0.00
2.0	11.5	11.6	0.87
10.0	12.7	12.7	0.00
20.0	12.6	12.7	0.79
40.0	12.2	12.6	3.28
84.0	11.3	12.1	7.08
1240.	4.30	8.76	104.

Table 4.8 Standard 250. micron cells without albedo illumination and 50. micron cells with albedo illumination at EOL.

THIN STANDARD CELL EOL OUTPUT POWER			
ρ (Ω–cm)	Standard Cell Without Albedo($\frac{mW}{cm^2}$)	Thin Standard With Albedo($\frac{mW}{cm^2}$)	Percent Gain(%)
1.0	10.3	10.4	0.97
2.0	11.5	12.0	4.35
10.0	12.7	15.1	18.9
20.0	12.6	16.2	28.6
40.0	12.2	16.9	38.5
84.0	11.3	17.4	54.0
1240.	4.30	18.5	330.

Table 4.9 Standard 250. micron cells without albedo illumination and tandem junction cells with albedo illumination at EOL showing improvement with albedo illumination.

TANDEM CELL EOL OUTPUT POWER			
ρ (Ω–cm)	Standard Cell Without Albedo($\frac{mW}{cm^2}$)	Tandem Cell With Albedo($\frac{mW}{cm^2}$)	Percent Gain(%)
1.0	10.3	11.7	13.6
2.0	11.5	12.0	4.35
10.0	12.7	14.2	11.8
20.0	12.6	14.4	14.3
40.0	12.2	14.5	18.9
84.0	11.3	13.9	23.0
1240.	4.30	6.02	40.0

Table 4.10 Standard 250. micron cells without albedo illumination and etched multiple vertical junction cells with albedo illumination at EOL showing improvement with albedo illumination.

EMVJ CELL EOL OUTPUT POWER			
ρ (Ω—cm)	Standard Cell Without Albedo($\frac{mW}{cm^2}$)	EMVJ Cell With Albedo($\frac{mW}{cm^2}$)	Percent Gain(%)
1.0	10.3	12.9	25.2
2.0	11.5	14.4	25.2
10.0	12.7	16.1	26.8
20.0	12.6	16.4	30.2
40.0	12.2	15.8	29.5
84.0	11.3	14.5	28.3
1240.	4.30	5.45	26.7

CHAPTER 5

CONCLUSIONS

This work has shown that the best cells for collection of albedo-generated carriers at EOL are the EMVJ cell and the high resistivity, thin standard cells. Tables 4.6-4.9 printed the EOL output power of each cell with and without albedo illumination as well as the percent gain in output power for all resistivities. Each cell except the 250. micron standard provided improvement in output power over a cell without albedo illumination. The tandem junction cell demonstrated some improvement over the standard cell, but not enough to merit use.

For all 250. micron cells, with or without albedo, the peak performance as a function of resistivity is in the 10. to 40. Ω–cm range. Lower resistivity cells suffer from excessive minority carrier diffusion length degradation. Higher resistivity cells suffer from a lack of conductivity modulation especially when the albedo is dark. Lack of conductivity modulation is overcome by reducing the thickness of standard cells. Thin standard cell efficiencies peaked at the highest base resistivity modeled.

Before running the simulations, steps were taken to carefully model the albedo spectrum and the degradation of the minority carrier diffusion length. Albedo is modeled as AM1.5 at 30.% of AM0.0 intensity (40. milliwatts/cm^2). The diffusion length degrades according to:

$$\frac{1}{L_n^2} = \frac{1}{L_o^2} + K_l(\rho)\Phi \qquad (5.1)$$

and values for $K_l(\rho)$ are found in the literature. Using equation 5.1 given $K_l(\rho)$ and L_o, L_n is calculated for any given incident equivalent fluence of 1.0MeV electrons. EOL is chosen as 1.0e15 1.0MeV electrons/cm^2 to be consistent with most published literature.

This work shows that definite improvement in cell output power at the peak of albedo illumination is possible by collection of albedo-generated carriers. The most efficient cell with albedo illumination (the 1240. Ω–cm thin, standard cell) provides 45.7% more power than the most efficient cell (10. Ω–cm standard cell) without albedo illumination. However, the albedo is present only half the time, and most of this time it is less than 40. milliwatts/cm^2. Therefore, the average output power gained during an orbit will be less than the gain at peak albedo illumination. Because of this, the time albedo light is available must be considered before selecting a cell for operation.

5.2 Recommendations

5.2.1 Evaluation of Surface Recombination Velocities

Data for surface recombination velocities of irradiated solar cells is needed to accurately model space solar cells. The surface recombination velocities, S_p and S_n, of a solar cell are significant in determining the exact efficiency of a cell. In the SCAP2D simulations S_p and S_n are found

according to:

$$S = \frac{C}{\tau_n} \tag{5.2}$$

where C = 1.0 centimeter. This formula makes sense in that a degraded lifetime as a result of irradiation is consistent with a higher surface recombination velocity (Section 3.7).

Lower energy radiation tends to increase S more than high energy radiation. Damage from one radiative particle tends to centralize at the point where the particle stops in the semiconductor [10]. Therefore, lower energy particles cause damage nearer the surface since they not penetrate as deeply. So any data on surface recombination velocities must include lower energy irradiation, not just 1.0MeV electrons. Data of this sort was not found, so equation 5.2 was developed as the nearest approximation. A relationship for S_n and S_n as a function of fluence much like equation 5.1 for diffusion length would be helpful.

5.2.2 Texturizing the Albedo-incident Surface

Although at least some albedo light is incident half the time, much of this is lost because of reflection. As the angle Θ of figure 2.1 increases, more of the albedo light is reflected. Antireflective coatings will improve the absorption some, but still too much light is lost to reflection.

Texturing the albedo surface improves the absorption of light incident on the back side. Texturing has been shown to reduce the reflectivity of bare silicon significantly [18]. This was shown for normally incident light. Since the albedo light can be incident at an oblique angle, texturing will improve the absorption even more for this application. Sater [15] found that texturizing the front side can hurt efficiency of front-illuminated cells because absorption of infrared illumination is enhanced, raising the operating temperature of the cell. Texturizing the back side enhances infrared absorption as the light will be internally reflected at the back surface. Although texturizing the albedo side of the cell can reduce the efficiency of the cell by raising the operating temperature, the gain in increased absorption of albedo illumination should outweigh this problem.

LIST OF REFERENCES

1. J.L. Gray, *Two-Dimensional Modeling of Silicon Solar Cells,* Ph.D. Thesis, Purdue University, West Lafayette,IN (August 1982).

2. F.M. Smits, "The Degradation of Solar Cells Under Van Allen Radiation", *IEEE Transactions on Nuclear Science,* NS-10 pp. 88-96, January 1963.

3. G. Strobl, et. al., "Bifacial Space Silicon Solar Cell", *Seventeenth IEEE Photovoltaic Specialists Conference* pp. 454-457 (1985).

4. D.M. Caughey and R.E. Thomas, "Carrier Mobilities in Silicon Empirically Related to Doping and Field," *Proceedings IEEE* 55, pp. 2192-2193 (1967).

5. B.E. Anspaugh and R.G. Downing, "Damage Coefficients and Thermal Annealing of Irradiated Silicon and GaAs Solar Cells", *Fifteenth IEEE Photovoltaic Specialists Conference* p. 499 (1981).

6. H.Y. Tada, and J.R. Carter, Jr., *Solar Cell Radiation Handbook,* Third Edition, JPL Publication 82-69, November 1982.

7. J.R. Srour, et. al., "Electron and Proton Damage Coefficients In Low-Resistivity Bulk Silicon and Silicon Solar Cells", NASA Report No. TM-X-3326 (1975). Northrop Research and Technology Center, Hawthorne, CA 90250.

8. I. Weinberg, et. al., "Performance of High Resistivity N+PP+ Silicon Solar Cells Under 1.0MeV Electron Irradiation" *Fifteenth IEEE Photovoltaic Conference.* p. 484 (1981).

9. Harold J. Hovel, *Semiconductors and Semimetals, Volume 2, Solar Cells,* New York, Academic Press Inc., 1975.

10. W. Rosenzweig, "Diffusion Length Measurements by Means of Ionizing Radiation", *Bell Systems Technical Journal,* vol. 41, no. 5, pp. 1573-1588, 1962.

11. A. Meulenberg, Jr., "Damage in Silicon Solar Cells From 2 to 155 MeV Protons", *Tenth IEEE Photovoltaic Specialists Conference* p. 359 (1973).

12. B.L. Sater (Personal Communication).

13. D.J. Roulston, N.D. Arora, and S.G. Chamberlain, "Modeling and Meaurement of Minority-Carrier Lifetime versus doping in Diffused Layers of N+-P Silicon Diodes," *IEEE Trans. on Electron Devices,* ED-29(2), pp. 284-291 (February 1982).

14. R.J. Schwartz, M.S. Lundstrom, and R.D. Nasby, "The Degradation of High Intensity BSF Solar Cell Fill Factors Due to a Loss of Base Conductivity Modulation", *IEEE Transactions Electron Devices,* ED-28 pp. 264-269, March 1981.

15. I. Weinberg, C.K. Swartz, and C. Goradia, "Radiation Damage In High-Resistivity Silicon Solar Cells",NASA Report #cp2408,E2706-18.

16. S.M. Sze, *Physics of Semiconductor Devices.* Second Edition. New York, John Wiley and Sons, Inc. 1981.

APPENDICES

A. Solar Cell Analysis Program in Two Dimensions

To effectively measure the effect of a specific parameter of a solar cell on its output characteristics, one must be sure that all other physical parameters remain constant. This makes effective comparison of solar cells difficult. Under laboratory conditions it is rarely possible to change one physical parameter and be assured that all other parameters remain constant. So to quantitatively measure the effect on efficiency and radiation hardness of a solar cell parameter such as base doping, idealy one would like to build a series of cells in which all other aspects of the cells remain unchanged. SCAP2D allows such comparison since all parameters remain constant for a series of computer simulations for which the base doping can be varied. The effect of any cell parameter is measured quantitatively in this way because it is assured that all other factors do not change in the code.

SCAP2D is a FORTRAN program that solves simultaneously the three semiconductor equations, the hole and electron continuity equations and Poisson's equation in two dimensions for hole and electron concentrations and the potential. These equations are solved at each node point for a mesh of nodes as shown in figure A.1. The cell in this figure is a unit cell. It is the smallest representation of the larger solar cell that is equivalent to modeling the entire cell. Nodes are located where the lines cross within the cell and on its boundary. These node positions are determined by the user and are concentrated in regions where the potential or carrier concentrations

change rapidly. The equations are solved using finite difference techniques.

Typical analytical models are incorporated in SCAP2D. Recombination is determined using Auger (A_n = 2.8e—31 and A_p = 9.9e—32) and Shockley-Read-Hall mechanisms with a single trap level assumed at the mid-gap. Slotboom-Degraaf bandgap narrowing is incorporated for high doping effects. Contacts are assumed to be ideal, and they are a source of shadowing for the incident surface. There is zero reflectance at both incident surfaces. No back surface reflector is used. Bulk doping is assumed constant and diffusions are calculated using error function complements given the surface concentration and junction depth.

Lifetimes are a part of the input deck of a SCAP2D run, and are recalculated with position as a function of the total doping at each node point (equations 4.1 and 4.2). τ_n and τ_p are given differing values to account for differing damage coefficients associated with P-type and N-type silicon. (This is described in more detail in radiation chapter--see section 3.6.4) Illumination spectrums are AM0.0 for sun light and AM1.5 for albedo light (Described in more detail in section 2.1).

The output of SCAP2D allows the user to see into the device under specific biases such as in figures 4.13 and 4.14 where the electron concentrations are plotted for a line within the cell. Quantities such as recombination rates, mobility, potential, carrier concentrations, and bandgap narrowing are available for every node under any specified applied voltage. Recombination percentages for every region (base, P+, N+, surfaces, or contacts) are produced to isolate the significant carrier loss regions. Finally, J_{sc}, V_{oc}, fill factor, collection efficiency, efficiency, and

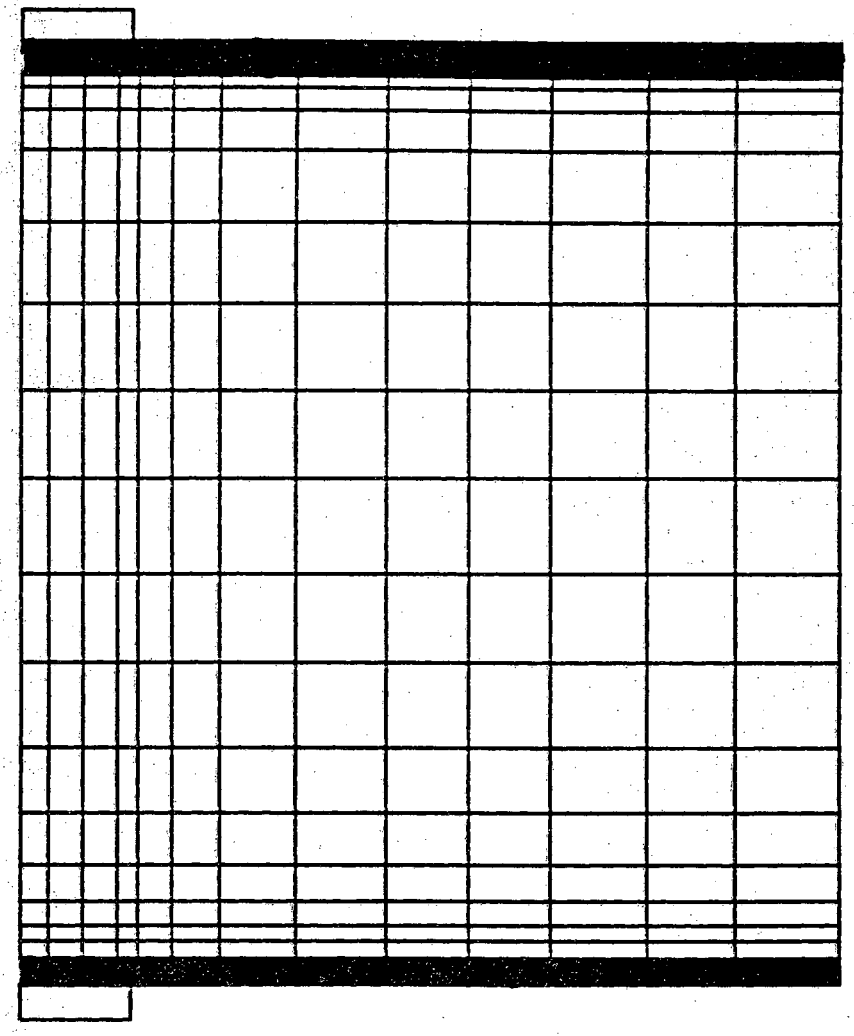

Figure A.1 Mesh of a simulated unit cell.

active area efficiency are computed for every run.

B. Comparisons of Simulation and Laboratory Data

Plots B.1 and B.2 show comparisons between SCAP2D simulation data and laboratory data. The solid lines in the graphs show output parameters of cells irradiated with 1.0 MeV electrons and illuminated with a solar simulator. The asterisks show SCAP2D simulations for the appropriate fluence of the cells. The cells were described as 200. micron cells with a BSF. No other information with regard to geometric parameters was given. The cells modeled are the same as those standard cells pictured in figure 1.1 and described by table 1.1 with two differences. The cell thickness at 200. microns is the only difference in geometry while τ_o, the initial lifetime, is 10. microseconds rather than 100. like the cells modeled for this work. This change in τ_o allowed better agreement with the low fluence part of the curves. No albedo light is incident for any of the cells.

C. Possible Sources of Error in the Simulations

Several assumptions must be made to model solar cells and their output parameter degradation with SCAP2D. Each assumption introduces error, and it is the purpose of this appendix to discuss these sources of error.

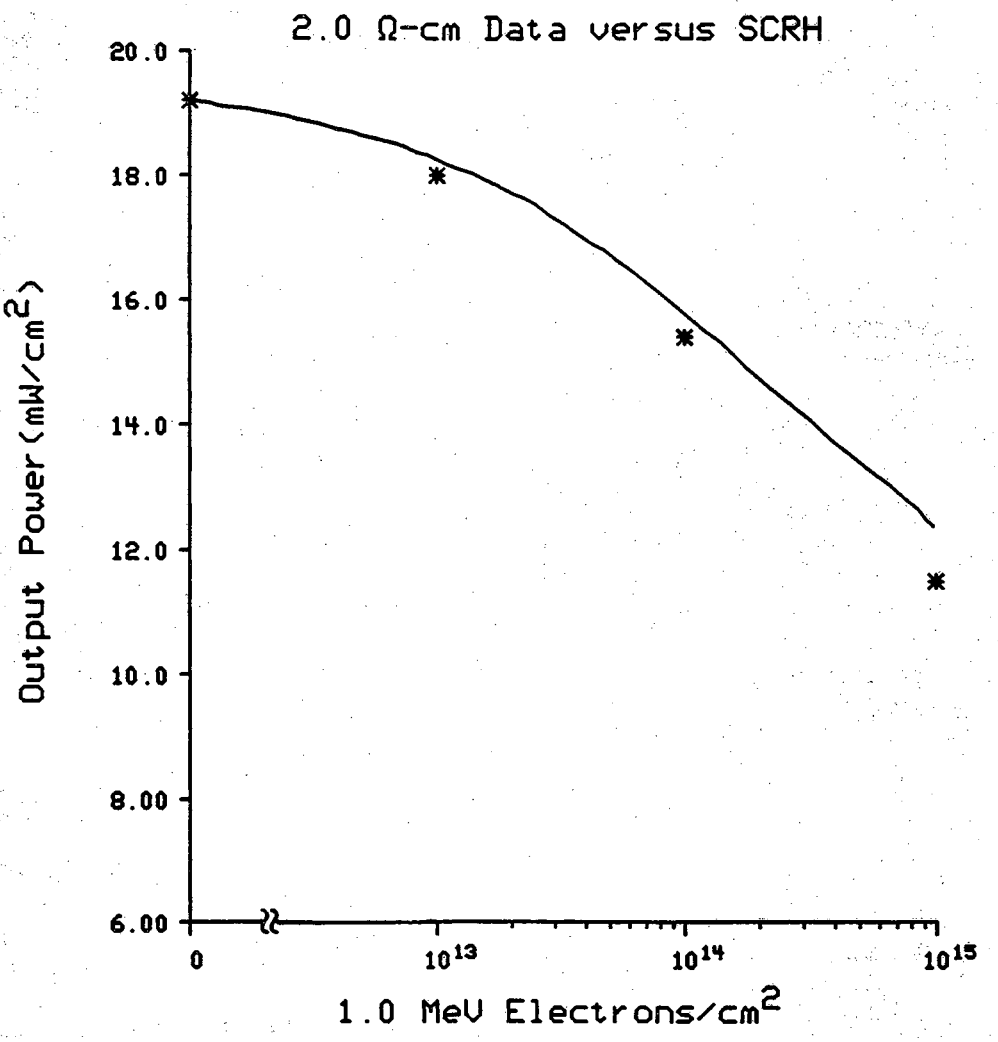

Figure B.1 Comparison of laboratory maximum power data (from Solar Cell Radiation Handbook[6]) versus SCAP2D simulations for 2.0 Ω—cm cells.

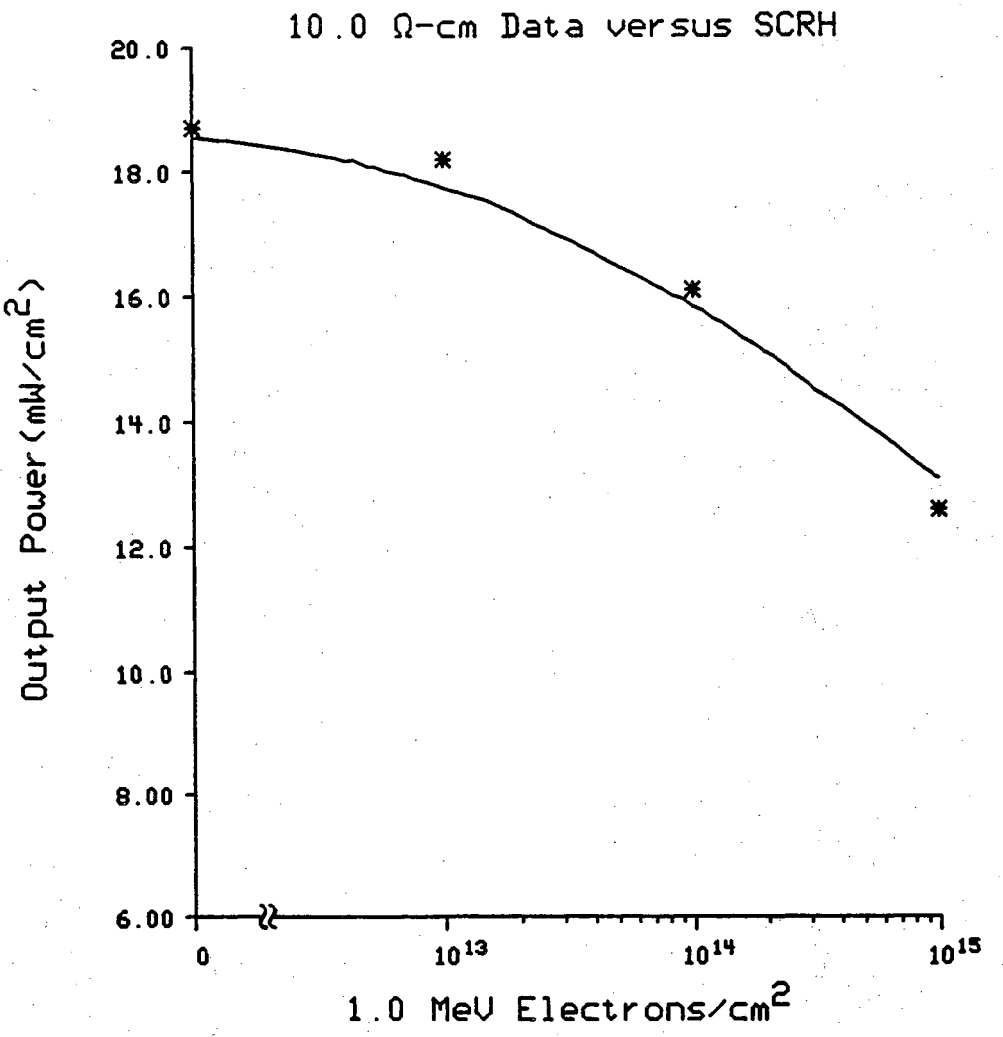

Figure B.2 Comparison of laboratory maximum power data (from Solar Cell Radiation Handbook[6]) versus SCAP2D simulations for 10. Ω–cm cells.

C.1 Diffusion length error from uncertainty in $K_l(\rho)$.

Uncertainty in the values found for the damage coefficient, $K_l(\rho)$, creates error in the calculation of lifetimes used for each solar cell run. For each resistivity cell, $K_l(\rho)$ is determined using an equation for a line that best fits the data found from literature. Since this is not a precise value for $K_l(\rho)$, error in the calculation of the diffusion length, L_n, in terms of $K_l(\rho)$ and the incident fluence occurs. Determination of the magnitude of that error is necessary to discover its effect on the accuracy of the cell simulations.

The electron diffusion length is determined by the following equation:

$$\frac{1}{L^2} = \frac{1}{L_o^2} + K_l(\rho)\Phi \tag{C.1}$$

where L_o is the original diffusion length after Φ radiation and $K_l(\rho)$ is the damage coefficient. Error in L_n is incurred because of error in L_o, incident fluence, and $K_l(\rho)$ and is computed as follows:

$$\sigma_{L_n} = \sigma_{K_l}\frac{\partial L_n}{\partial K_l} + \sigma_{\Phi}\frac{\partial L_n}{\partial \Phi} + \sigma_{L_o}\frac{\partial L_n}{\partial L_o} \tag{C.2}$$

where σ is the uncertainty in the quantity corresponding to the specific subscript. Since all cells have the same beginning lifetimes (100. microseconds before SCAP2D recomputes τ with equations 4.1 and 4.2), and are modeled at the same levels of incident fluence, L_o and the incident fluence are assumed to be correct. Equation C.2 reduces to C.3.

$$\sigma_L = \sigma_{K_l} \frac{\partial L}{\partial K_l} \tag{C.3}$$

Taking the derivative of L with respect to K_l leaves C.4 as the error in L_n.

$$\sigma_L = \sigma_{K_l} L_o^3 \frac{\Phi}{2(1 + L_o^2 K_l \Phi)^{\frac{3}{2}}} \tag{C.4}$$

Table C.1 Error in L_n as a function of fluence for K_l =1.0e-9 particles^{-1}.

L_o =600. microns K_l = 1.0e-9		
Fluence($\frac{e}{cm^2}$)	L(μm)	Error(μm)
1.0e13	98.6	9.60
1.0e14	31.5	3.15
1.0e15	10.0	1.00

Tables C.1-C.3 show values of error in microns for L_n as a function of K_l and increasing radiative fluence. A possible error of 20% is assumed for K_l

Table C.2 Error in L_n as a function of fluence for K_l =1.0e-10 particles^{-1}.

L_o =600. microns K_l = 1.0e-10		
Fluence($\frac{e}{cm^2}$)	L(μm)	Error(μm)
1.0e13	280.	21.9
1.0e14	98.6	9.60
1.0e15	31.6	3.15

Table C.3 Error in L_n as a function of fluence for K_l =1.0e-11 particles^{-1}.

L_o =600. microns K_l = 1.0e-11		
Fluence($\frac{e}{cm^2}$)	L(μm)	Error(μm)
1.0e13	514.	13.6
1.0e14	280.	21.9
1.0e15	98.6	9.60

in this table. The greatest error in L_n is 10%; this occurs many times. The current of an ideal photodiode with an abrupt junction is:

$$J = q\left[\frac{D_n}{L_n}\frac{n_i^2}{N_A} + \frac{D_p}{L_p}\frac{n_i^2}{N_D}\right](e^{\frac{qV_A}{kT}} - 1) - qG_l[L_p + L_n] \qquad (C.5)$$

where G_l is a constant generation rate throughout the device. J_{sc} is:

$$J_{sc} = -qG_l[L_p + L_n] \qquad (C.6)$$

Using 10% error in L_n for this circumstance results in 10% uncertainty in J_{sc}. However, the generation rate in cells is an exponentially decreasing function of distance from the light-incident surface. Therefore, error in J_{sc} as a result of uncertainty in L_n changes with the magnitude of L_n as well as the geometry of the device. The most significant uncertainty is encountered with standard cells with L_n comparable to the thickness of the cell. The albedo-generated carriers are mostly generated near the back surface of the cell. So when L_n is comparable to the cell thickness, the greatest number of carriers are on the borderline of being collected or not being collected. This is not a significant problem for the tandem junction and EMVJ cells owing to their albedo side collecting junctions. For these cells, more error is seen for smaller L_n because of the same principle. As L_n degrades, the local generation rate at the distance L_n from the collecting junctions (front or albedo side) increases so that, again, more carriers are on the borderline of

being collected or being annihilated through recombination before reaching the junction.

For most cells, this worst case error in J_{sc} will be less than 10%. Error in V_{oc} will be less since it is a function of the natural log of J_{sc}. Most of the generation of carriers occurs within 10. microns of the light incident surface. So as long as L_n is not comparable to the cell thickness and is not less than 10. microns, the error in J_{sc} as a result of uncertainty in $K_l(\rho)$ will be small and confidence in the trend shown by the simulations is justified.

C.2 Selection of Initial Cell Lifetime

Clearly the choice of τ_o, the cell lifetime before irradiation, determines the efficiency of operation for low levels of fluence. However, the lifetime dependence on τ_o diminishes as Φ increases. The length of time that τ is dependent on τ_o is determined by the magnitude of $K_l(\rho)$. Figure C.1 shows lifetimes versus fluence for 1.0, 20., and 1240. Ω—cm cells for τ_o equal to 100. and 10. microseconds. For lower resistivity cells, the two plots join more quickly and show little change in the EOL lifetimes. The 1240. Ω—cm base lifetimes differ throughout the life of the cell. In order to accurately simulate the laboratory data in A.1, τ_o is reduced to 10. microseconds. This casts some doubt as the validity of the choice of 100. microseconds as the initial lifetime of the modeled cells. If indeed τ_o=100. microseconds is too high, the result will be that higher resisitivity cells will produce higher efficiencies throughout life.

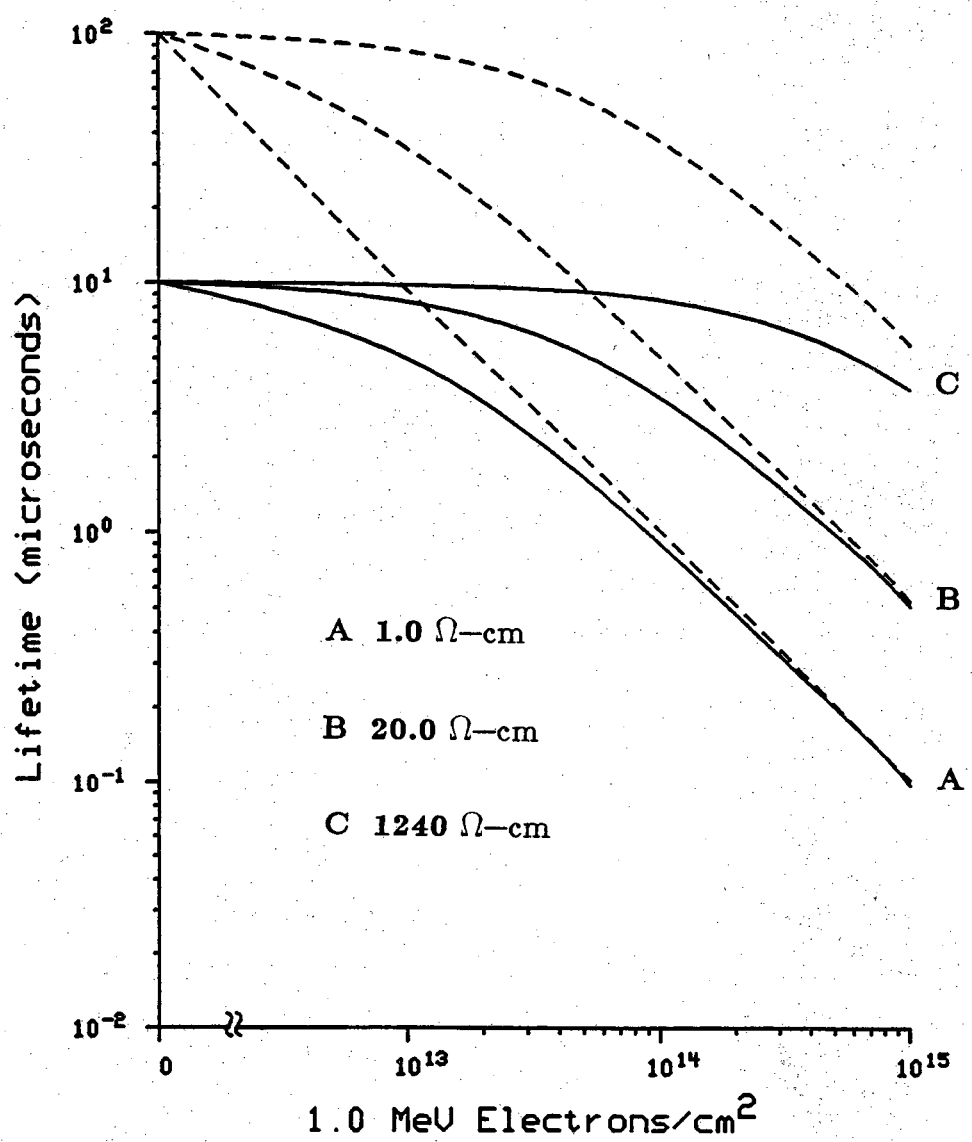

Figure C.1 Lifetimes versus fluence for 1.0, 20. and 1240. Ω–cm cells for τ_o= 100. and 10. microseconds.

C.3 Possible Problems With The Models

There are two factors in the model of degradation that need additional consideration before performing simulations. First, computation of the base lifetime neglects the BSF. This field is highly doped P-type, and as such will have a much higher $K_l(\rho)$. So the radiation-degraded lifetime is, in reality, lower in this highly doped region than the model assumes. Thus, our recombination rates in the P+ region will be optimistic when compared to a real device. The error will be small though since the P+ region is small on the tandem junction and EMVJ cells and section 2.3.2 showed that the BSF is ineffective at EOL for standard cells.

No supportive data was found in the literature for the surface recombination rate model chosen.

$$S = \frac{C}{\tau_n} \tag{C.7}$$

Equation C.7 is a worst case approximation to the surface recombination rate for each cell. It affects each cell similarly with the exception of thin standard cells. This is discussed in more detail in section 3.7. Table 3.1 shows EOL surface recombination for each cell type and resistivity. The EMVJ and tandem junction cells show higher S because of the small region on the albedo side where there is no surface-normal electric field.

D. Lifetimes Used in SCAP2D Modeling

These tables list the cell lifetimes, base minority carrier diffusion lengths, and surface recombination velocities for all the cell resistivities modeled in this work. The N-type emitter damage coefficient for P-type base solar cells is 3.0e-8 [12], and the P-type emitter for the N-type base cell is found by extending the empirical equation to the doping used ($1.0e19/cm^3$) although the data doesn't cover this region. The lifetimes listed are the values input into SCAP2D.

Table D.1 1.0 Ω–cm N-type solar cell.

1.0 Ω–cm N–type $K_l = 2.6e-9$				
Fluence($\frac{e}{cm^2}$)	$\tau_n(\mu S)$	$\tau_p(\mu S)$	$L_p(\mu m)$	S(cm/s)
0.0	100.	100.	349.	1.0e4
1.0e13	6.35	3.06	61.1	3.26e5
3.16e13	2.10	0.988	34.7	1.01e6
1.0e14	0.674	0.315	19.6	3.17e6
3.16e14	0.214	0.0997	11.0	1.0e7
1.0e15	.0678	0.0316	6.20	1.0e7

Table D.2 1.0 Ω–cm P-type solar cell.

1.0 Ω–cm P–type $K_l = 3.09e{-}10$				
Fluence($\frac{e}{cm^2}$)	$\tau_n(\mu S)$	$\tau_p(\mu S)$	$L_n(\mu m)$	S(cm/s)
0.0	100.	100.	560.	1.0e4
1.0e13	9.36	1.84	171.	1.07e5
3.16e13	3.16	0.588	99.6	3.17e5
1.0e14	1.02	0.187	56.6	9.78e5
3.16e14	0.325	0.0591	31.9	3.08e6
1.0e15	0.103	0.0187	18.0	9.69e6

Table D.3 2.0 Ω—cm P-type solar cell.

2.0 Ω—cm P—type $K_l = 2.06e{-}10$				
Fluence($\frac{e}{cm^2}$)	$\tau_n(\mu S)$	$\tau_p(\mu S)$	$L_n(\mu m)$	S(cm/s)
0.0	100.	100.	576.	1.0e4
1.0e13	12.8	1.84	206.	7.82e4
3.16e13	4.44	0.588	121.	2.25e5
1.0e14	1.45	0.187	69.2	6.92e5
3.16e14	0.462	0.0591	39.1	2.16e6
1.0e15	0.146	0.0187	22.0	6.83e6

Table D.4 10.0 Ω—cm P-type solar cell.

10.0 Ω—cm P—type $K_l = 8.0e{-}11$				
Fluence($\frac{e}{cm^2}$)	$\tau_n(\mu S)$	$\tau_p(\mu S)$	$L_n(\mu m)$	S(cm/s)
0.0	100.	100.	589.	1.0e4
1.0e13	26.5	1.84	303.	3.78e4
3.16e13	10.2	0.588	188.	9.79e4
1.0e14	3.48	0.187	110.	2.88e5
3.16e14	1.13	0.0591	62.5	8.89e5
1.0e15	0.359	0.0187	35.3	2.79e6

Table D.5 20.0 Ω–cm P-type solar cell.

20.0 Ω–cm P–type $K_l = 5.3e-11$				
Fluence($\frac{e}{cm^2}$)	$\tau_n(\mu S)$	$\tau_p(\mu S)$	$L_n(\mu m)$	S(cm/s)
0.0	100.	100.	592.	1.0e4
1.0e13	34.9	1.84	350.	2.87e4
3.16e13	14.5	0.588	225.	6.89e4
1.0e14	5.09	0.187	134.	1.97e5
3.16e14	1.67	0.0591	76.4	5.99e5
1.0e15	0.533	0.0187	43.2	1.88e6

Table D.6 40.0 Ω—cm P-type solar cell.

40.0 Ω—cm P—type $K_l = 3.5e-11$				
Fluence($\frac{e}{cm^2}$)	$\tau_n(\mu S)$	$\tau_p(\mu S)$	$L_n(\mu m)$	S(cm/s)
0.0	100.	100.	593.	1.0e4
1.0e13	44.5	1.84	396.	2.25e4
3.16e13	20.2	0.588	267.	4.94e4
1.0e14	7.43	0.187	162.	1.35e5
3.16e14	2.48	0.0591	93.3	4.04e5
1.0e15	0.796	0.0187	52.9	1.26e6

Table D.7 84.0 Ω—cm P-type solar cell.

84.0 Ω—cm P—type $K_l = 2.29e-11$				
Fluence($\frac{e}{cm^2}$)	$\tau_n(\mu S)$	$\tau_p(\mu S)$	$L_n(\mu m)$	S(cm/s)
0.0	100.	100.	593.	1.0e4
1.0e13	55.3	1.84	441.	1.81e4
3.16e13	28.2	0.588	315.	3.55e4
1.0e14	11.0	0.187	197.	9.08e4
3.16e14	3.77	0.0591	115.	2.65e5
1.0e15	1.22	0.0187	65.6	8.18e5

Table D.8 1240.0 Ω—cm P-type solar cell.

1240.0 Ω—cm P—type $K_l = 4.7e{-}12$				
Fluence($\frac{e}{cm^2}$)	$\tau_n(\mu S)$	$\tau_p(\mu S)$	$L_n(\mu m)$	S(cm/s)
0.0	100.	100.	594.	1.0e4
1.0e13	85.7	1.84	550.	1.17e4
3.16e13	65.5	0.588	481.	1.53e4
1.0e14	37.5	0.187	364.	2.67e4
3.16e14	16.0	0.0591	237.	6.27e4
1.0e15	5.66	0.0187	141	1.77e5